The effect of rainfall variability on Nitrogen dynamics

in a small agricultural catchment

- 3 Qiaoyu Wang^{1, 3}, Jie Yang^{1, 2}, Ingo Heidbüchel^{4, 5}, Teng Xu^{1, 3}, Chunhui Lu^{1, 2}
- 4 ¹The National Key Laboratory of Water Disaster Prevention, Hohai University,
- 5 Nanjing, China
- 6 ²College of Hydrology and Water Resources, Hohai University, Nanjing, China
- 7 ³College of Water Conservancy and Hydropower Engineer, Hohai University,
- 8 Nanjing, China
- 9 ⁴UFZ Helmholtz-Centre for Environmental Research GmbH, Department of
- 10 Hydrogeology, Leipzig, Germany
- 11 5Hydrologic Modeling Unit, Bayreuth Center of Ecology and Environmental
- 12 Research (BayCEER), University of Bayreuth, Bayreuth, GermanyHochschule
- 13 Koblenz, Koblenz, Germany
- 14 Correspondence to: Jie Yang (yangj@hhu.edu.cn); Chunhui Lu (clu@hhu.edu.cn)

Abstract. Throughout history, extreme storms and droughts have had serious impacts on society and ecosystems globally. Rainfall variability particularly has been identified as a primary manifestation of climate change. However, so far little has been done to explore the effect of rainfall variability on water quality. This study aims to investigating investigate the effect of rainfall variability on nitrogen (N) dynamics and its potential influence on water quality. The transport of water and nitrate was simulated for a small agricultural catchment in Central Germany using the fully coupled surface-subsurface model HydroGeoSphere. Rainfall time series with specific climatic characteristics were generated using a stochastic rainfall generator. N transformation and transport were compared for four scenarios (with high, normal, low annual precipitation, and low annual precipitation wet, normal, dry and extremely dry conditions coupled with reduced plant uptake, respectively) in order to identify the impact of inter-annual rainfall variability. The results suggest that higher annual precipitation enhances N transformation and transport, whereas lower annual precipitation is conducive to the N retention capacity. Nonetheless, *The retention capacity declines severely when vegetation suffers from drought stress, suggesting that vegetation plays a vital role in the response of N dynamics under to extreme droughts. The linear regressions between selected parameters of the rainfall generator and N loads/fluxes were analyzed to elucidate the impact of intra-annual rainfall variability. The results indicate that wet/dry conditions and different dry-wet patterns caused by storm duration distributions and inter-storm period distributions can significantly affect N loads and in-stream nitrate concentration, respectively. In the warm season, droughts prompt the accumulation of soil organic nitrogen (SON), but drying-wetting cycles can enhance the extensive transformation of SON. In-stream nitrate concentration dramatically elevates during the rewetting period after athe drought. Wet/dry conditions and patterns of precipitation intensity within a year determined by seasonal average rainfall intensity and the probability of drizzle events prominently alter mineralization and plant uptake. Elevated mean rainfall intensity has merely a small effect on stream water quality. Therefore, mineralization and plant uptake are critical processes governing N dynamics and the impact of nitrate on water quality under varying rainfall conditions. Overall, the study clarifies the effect of rainfall variability on N dynamics in a small agricultural catchment, which provides theoretical support for formulating fertilization strategies and protecting aquatic ecosystems under climate change.

15

16

17

18

19

20

21

22

23

24

25

26

27

28

29

30

31

32

33 34

35

36

37

38

39

40

41

42

43

44

45

46

47

48

49

50

Key Points: N dynamics, HydroGeoSphere, Rainfall variability, Stochastic rainfall generator

1 Introduction

51

52 The hydrological processes are susceptible to meteorological conditions on various 53 spatial and temporal scales [Ionita et al., 2017; Laaha et al., 2017; Zhang et al., 2021]. 54 In the past decades, extreme climate events intensified by human-induced climate 55 change have frequently occurred globally [Pall et al., 2011; Min et al., 2011; Williams 56 et al., 2015; Hari et al., 2020], most of which caused water scarcity and poor water 57 quality at regional scales [Zwolsman and van Bokhoven, 2007; Delpla et al., 2009; 58 Whitehead et al., 2009; Stahl et al., 2016; Ballard et al., 2019; Bauwe et al., 2020; 59 Geris et al., 2022]. As predominant extreme climate events worldwide, hHeavy 60 rainstorms and severe droughts being the predominant extreme climate events around 61 the globe share the a common characteristic of rainfall variability [Trenberth et al., 62 2011; Pendergrass et al., 2017; Hanel et al., 2018]. In the context of global warming 63 scenarios, anthropogenic amplification of rainfall variability has been identified 64 [Zhang et al., 2024]. Thus, the effect of rainfall variability on water resources has 65 attracted much attention around the world. During heavy rainstorms, extraordinary rainfall amounts and intensities cause large 66 amounts of rainwater to infiltrate into soils and trigger flash floods in a short time. 67 68 Increased groundwater flow and enhanced surface runoff stimulate the movement of 69 solutes retained in the soil, which thereby can lead to water quality degradation [Geris 70 et al., 2022]. Different from heavy rainstorms, severe droughts driven by precipitation 71 deficits occur during several months and potentially yearsneed to take several months 72 or potential years to reach their full intensity [Otkin et al., 2018], from which it takes 73 1-2 years for hydrological components to recover [Hanel et al., 2018]. Wilusz et al. 74 [2017] decomposed the relationship between rainfall variability and transit times, a 75 reflection of water velocities that control solute transport, and illustrated that climate 76 change may seasonally alter the ages of water in streams and thereby influence water 77 quality in the future. 78 Nitrate (NO₃-N) is a major solute threatening the quality of drinking water and 79 destroying the structure and functions of aquatic ecosystems [Vitousek et al., 2009; Alvarez-Cobelas et al., 2008; Dupas et al., 2017]. The nitrate turnover processes 80 81 established at the catchment scale are expected to change due to climate change 82 [Whitehead et al., 2009; Hesse and Krysanova, 2016; Mosley, 2015], especially due to 83 increasing drought events [Zwolsman and van Bokhoven, 2007; Ballard et al., 2019; 84 Zhou et al., 2022; Winter et al., 2023]. Several extreme rainfalls events and droughts 85 occurred in Central Europe during the last two decades, which has attracted 86 widespread attention [Ulbrich et al., 2003; Fink et al., 2004; Orth, Vogel, Luterbacher, 87 Pfister, and Seneviratne, 2016; Thieken et al., 2016; Hanel et al., 2018; Hari et al., 88 2020; Voit, P. and Heistermann, M., 2024]. Notably, the 2018 event triggered 89 multiple species in Central European forests,

companied by unexpectedly persistent drought legacy effects [Schuldt et al., 2020].

Zhou et al. [2022] detected higher soil N surplus (total N input with the crop/plant uptake subtracted) and a decrease ind the terrestrial N export in agricultural areas located in Central Germany during the drought years (2015-2018). The same phenomenon reported in the Nitrate Report 2020 of the Netherlands (RIVM, 2021) indicates that more N was retained in the soil during the drought period compared to the pre-drought period. Notably, the 2018-2019 (consecutive) drought event triggered unprecedented tree mortality across multiple species in Central European forests, accompanied by unexpectedly persistent drought legacy effects [Schuldt et al., 2020]-However, by studying the 2018 2019 (consecutive) drought in Central Germany, from which Winter et al. [2023] drew the conclusion that severe multi-year droughts can reduce the nitrogen (N) retention capacity of catchments. These appear to be opposite conclusions They seem opposite conclusions, which can be attributed to the different investigation timescales. The former study compared N export between drought years and the pre-drought period. The latter study considered the subsequent rewetting period, when most nitrogen accumulated during the drought left the catchment. Leitner et al. [2020] also found that in the year after a summer drought, NO₃ leaching via soil water seepage was significantly elevated compared to the long-term mean in a temperate mixed forest on karst, which was investigated in wetland-influenced catchments as well [Watmough et al., 2004]. These studies demonstrate prove that rainfall variability has a profound ly impact on affects N dynamics at both inter-annual and intra-annual timescales. Therefore, it is imperative

91

92

93

94

95

96

97

98

99

100

101

102

103

104

105

106

107

108

109

110

to shed light on the impact of rainfall variability on water quality in terms of N dynamics.

112

113

114

115

116

117

118

119

120

121

122

123

124

125

126

127

128

129

130

131

To fill the gap, the present study explored the impact of rainfall variability on N dynamics and its potential influence on water quality across inter-annual and intra-annual timescales. To characterize rainfall variability, a stochastic rainfall generator [Robinson and Sivapalan, 1997] was employed to generate rainfall time series with different climatic characteristics. The research was conducted in a small agricultural catchment located in Central Germany, where a hydrological model was previously established utilizing the fully coupled surface-subsurface numerical simulator HydroGeoSphere [Yang et al., 2018]. The framework of N dynamics was modified from the ELEMeNT approach [Exploration of Long-tErM Nutrient Trajectories; Van Meter et al., 2017]. The research is divided into two main components. First, three representative years (with high, normal, and low annual precipitation amounts, respectively) were chosen from the past two decades in Central Germany as the target scenarios. A fourth scenario with low annual precipitation amounts coupled with reduced plant uptake represents a case where vegetation is partially destroyed by extreme droughts. The statistical analyses of N loads and fluxes and a comparison across different scenarios were conducted to reveal the influence of inter-annual rainfall variability. Second, rainfall time series generated using the stochastic rainfall generator by separately altering specific the rainfall-generator parameters <u>substitute</u> forwere used to <u>substitute</u> the rainfall data in the simulation period to drive the flow and nitrogen transport models. The responses of the N loads and fluxes to the parameters (e.g., the amplitudes of the seasonal variations in the storm duration and inter-storm period) were thoroughly analyzed to clarify the effect of intra-annual rainfall variability. The study will provide theoretical support for formulating fertilization strategies and protecting aquatic ecosystems in the context of climate change.

2 Data collection

2.1 Study Site

The studied catchment, Schäfertal, is located on the lower reaches of the eastern Harz Mountains, Central Germany, with an area of 1.44 km². Since 1968, this first-order catchment has been subject to broad hydrogeological investigations, analyses, and research [Altermann et al., 1970; Altermann et al., 1977; Borchardt et al., 1981; Altermann et al., 1994; Wollschläger et al., 2016]. The valley bottom contains riparian zones with pasture and a small channel (Figure 1a). The hillslopes on both sides of the channel have an average slope of 11°, mostly used as farmland. The farmland undergoes intensive agriculture, primarily winter wheat growing [Yang et al., 2018]. Two small portions near the western edge are mostly forest. The land use types generally remain stable unless economic and ecological goals change The types of land use in the catchment do not generally convert until the economic and ecological

goals vary between years, e.g., shifting between planting and pasture [Wang et al., 2023]. A meteorological station, which is 200 m from the catchment outlet, provides records of precipitation, air and soil temperatures, radiation, and wind speed. The catchment outlet in the stream, where a gauge station was built, is considered the sole exitis considered as the unique exit that allows water and solutes to leave the catchment and enter the downstream catchments. This is because a subsurface wall (~55 m long and ~7 m deep) was erected across the valley to block subsurface flow. The gauge station provides discharge data at 10-minute intervals, aggregated to daily means in this study. Nitrate concentration data were measured by sampling near the gauge station at 14-days to monthly intervals [Dupas et al., 2017], covering the period 2001-2010. The aquifer is thin, with the thickness varying from ~5 m near the valley bottom to ~2 m at the top of the hillslopes (I-I cross section, Figure 1a). Thirteen wells, each ~2 meters deep, were constructed and fitted with automated data loggers to record groundwater levels. The groundwater levels exhibit pronounced seasonal variations, rising to the land surface during winter and receding to depths of ~3 meters below the ground during summer. The groundwater storage is low (~500 mm, stored water volume divided by catchment area). Most of the groundwater converges towards the channel vicinity, with the upper sections of the hillslopes typically in an unsaturated state [Yang et al., 2018]. Luvisols and Gleyic Cambisols are the aquifer materials of the hillslope. The valley bottom is dominated by Gleysols and Fluvisols (Figure 1b)

152

153

154

155

156

157

158

159

160

161

162

163

164

165

166

167

168

169

170

171

[Anis and Rode, 2015]. Generally, the aquifer is comprised of two horizontal layers: a top layer of approximately 0.5 m thickness, with higher permeability, higher porosity, and the developed root zone from crops; and a base layer with less permeability due to the high loam content [Yang et al., 2018]. The bedrock underlying the aquifer is comprised of greywacke and shale [Graeff et al., 2009]. Owing to the aquifer material and unknown hydraulic properties, the bedrock is often regarded as impermeable.

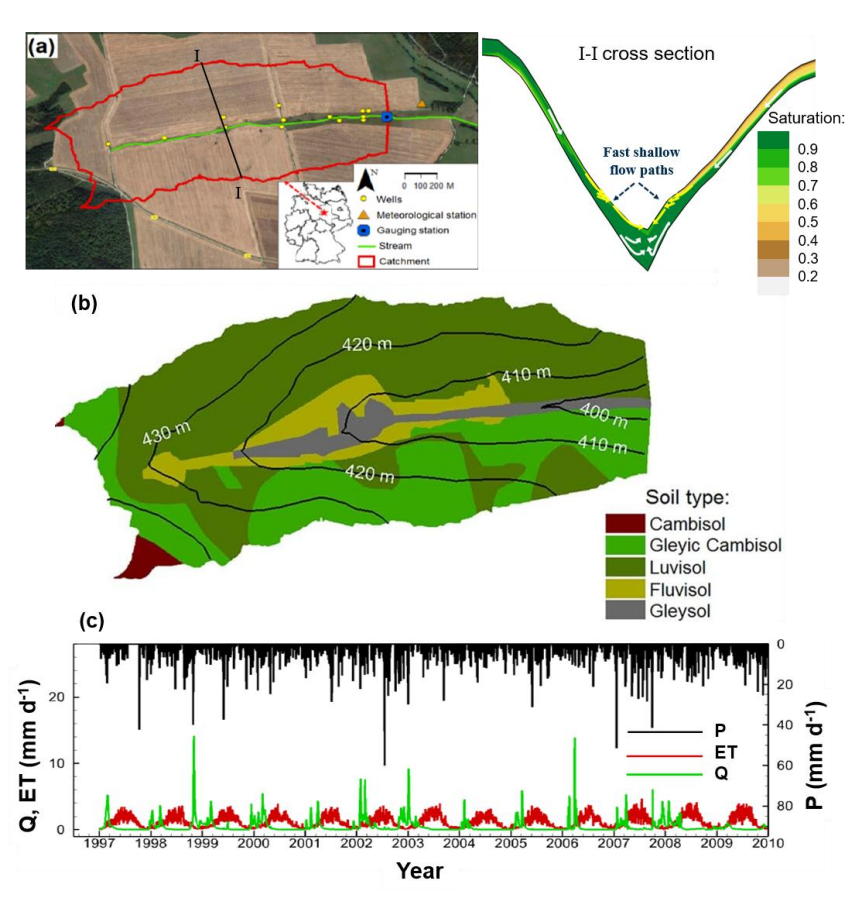


Figure 1. (a) The catchment 'Schäfertal' indicated by the red line (background image from © Google Maps), with a cross-sectional view for the flow and saturation [*Yang et al.*, 2018]. (b)

The distribution of soil type in the catchment. (c) The measured daily precipitation (P),

discharge (Q), and the simulated actual evapotranspiration (ET) [Yang et al., 2018].

2.2 Measured data

The studied catchment exhibits a temperate and humid climate with pronounced seasonality. The humid climate in wet regions is quantified by an aridity index of 1.0. The ET is the main driver of the hydrologic seasonality, as the precipitation is uniformly distributed across the year. According to the meteorological data records from 1997 to 2010, the mean annual precipitation (P) and discharge (Q) are 610 mm and 160 mm, respectively (Figure 1c). Based on the 14-year water balance (P = ET + Q), the actual mean annual evapotranspiration (ET) is 450 mm. The in-stream nitrate concentration (C_Q) was measured at fortnightly to monthly intervals [Dupas et al., 2017], covering the period 2001-2010. The N surplus, which is the annual amount of nitrogen remaining in the soil after the consumption by plant uptake from the external N input, was estimated as 48.8 kg N ha⁻¹ year⁻¹ during 1997–2010 for this catchment [Bach and Frede, 1998; Bach et al., 2011]. The C_Q and N surplus are used to calibrate the N transport model [Wang et al., 2023]. Adequate data from numerous investigations and previous research supports the exploration of N dynamics in the agricultural catchment.

3 Methodology

201 The hydrological model of Schäfertal catchment was established using

HydroGeoSphere [Therrien et al., 2010] in the previous study [Yang et al., 2018]. The framework of N dynamics [Yang et al., 2021], modified from the ELEMeNT modeling approach [Exploration of Long-tErM Nutrient Trajectories, Van Meter et al., 2017], was applied to track the fate of N in soil and groundwater in the present study. Based on the hydrological and transport model, the effect of topographic slope on the export of nitrate [Yang et al., 2022] and the spatial-temporal variation of nitrogen retention [Wang et al., 2023] were explored. In the present study, the two models were employed to investigate the effect of rainfall variability on N dynamics, for which rainfall time series with climatic characteristics, substituting for the precipitation data during the simulation period, were generated by a stochastic rainfall generator [Robinson and Sivapalan, 1997; Wilusz et al., 2017]. These models are described below.

3.1 Flow modeling

HydroGeoSphere is a 3D control volume finite element simulator that can model fully coupled surface-subsurface hydrological processes by the dual nodes approach. It can not only describe crucial hydrological processes such as dynamical evapotranspiration, snow, sublimation, snowmelt, and freeze and melt of pore water, but also simulate 2D overland flow by Manning's equation and the diffusive-wave approximation of the St. Venant equations, 3D variably saturated underground flow by Richards' equation and Darcy's law, flow in porous media, as well as the transport of reactive solutes. In

addition, HydroGeoSphere allows the simulation of 1D surface flow in a channel network and water exchange flux between the channel domain and the subsurface domain [Yang et al., 2015]. HydroGeoSphere has been frequently used to model catchment hydrological processes and solute transport in many previous studies [e.g., Therrien et al., 2010; Yang et al., 2018]. Please refer to Therrien et al. [2010] for the governing equations and technical details. The hydrological model of Schäfertal catchment is briefly recapitulated in the following. More details are provided in Yang et al. [2018]. In the model, the subsurface domain between the surface and bedrock was depicted using 3D prisms with side length ranging from 30 m to 50 m. The surface domain was filled by the uppermost 2D triangles of the generated 3D prismatic mesh, while the channel was delineated by 1D segments with specified widths and depths. According to different aquifer materials and the difference in their permeability in the vertical direction, the subsurface domain was separated into ten property zones with zonal hydraulic conductivity and porosity values. The surface domain and channel were parameterized with a Manning roughness coefficient representing the land use. Spatially uniform and temporally variable precipitation (Figure 1c) was applied to the entire surface domain. ET is computed as a combination of plant transpiration from the root zone and evaporation down to the evaporation depth [Therrien et al., 2010]. A critical depth boundary condition was assigned to the outlet in the channel domain to simulate the

222

223

224

225

226

227

228

229

230

231

232

233

234

235

236

237

238

239

240

241

a preliminary model run was performed for the period spanning 1997 to 2007. The simulated results at the end of the period were taken as initial conditions for the actual simulations.

Key parameters that significantly influence the hydrological processes were selected for the calibration [Anis and Rode, 2015; Graeff et al., 2009] using the software package PEST [Doherty and Hunt, 2010]. PEST uses the Marquardt method to minimize a target function by varying the values of a given set of parameters until the optimization criterion is reached. The groundwater levels measured in groundwater wells and the discharge measured at the gauging station were used as target variables. Considering high CPU time (~1 day to run the model for the period from 1997 to 2007), the calibration period spans 1 year, from October 2002 to October 2003. Subsequently, the calibrated model was verified by reproducing time-variable

3.2 Nitrogen transport in soil and groundwater

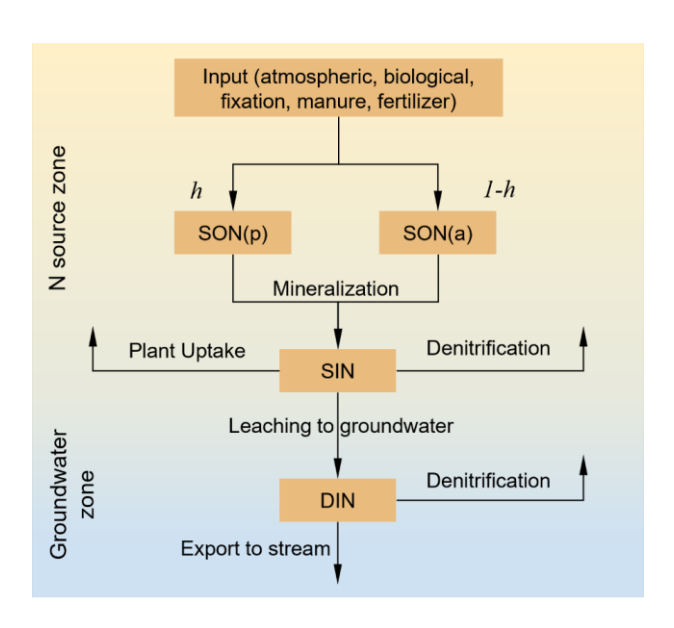
The transformation and transport of nitrogen in the <u>underground areasubsurface</u> are tracked by the framework of N dynamics modified from ELEMeNT. ELEMENT is a comprehensive model maintaining a landscape memory, that is, considering the effect of not only current conditions but also past land use and nutrient dynamics on current fluxes [Van Meter et al., 2017]. External nitrogen input goes through transformation and transport in the soil, and subsequently filters into groundwater, and gets exported

groundwater levels for the wells over the entire simulation period [Yang et al., 2018].

to the surface water body. Throughout the nitrogen cycle, various forms of nitrogen undergo complex biogeochemical processes.

The framework includes a N source zone forming in shallow soil and a groundwater zone (Figure 2). There are two assumptions in the N source zone: 1) the total N load in the N source zone is comprised of an organic N (SON) pool and an inorganic N (SIN) pool; 2) the external N input contributes only to the SON. The external N input represents atmospheric deposition, biological fixation, animal manure from the pasture area, and N fertilizer from the farmland. The SON is further distinguished as active SON with faster reaction kinetics and protected SON with slower reaction kinetics. Both SON(a) and SON(p) are transformed into SIN by mineralization. SIN is further consumed by plant uptake and denitrification, and leaches from soil to groundwater as dissolved inorganic N (DIN), representing mainly nitrate in the studied catchment [Yang et al., 2018; Nguyen et al., 2021]. DIN can further undergo denitrification until being exported to the stream. The framework is able to capture the main processes of nitrogen transformation and transport in soil and groundwater

[Yang et al., 2018].



279280

282

283

284

285

286

287

Figure 2. The framework simulating the transformation and transport of nitrogen in soil N source zone and groundwater zone, modified based on [Yang et al. 2021].

source zone and groundwater zone, modified based on [Yang et al., 2021].

The governing equations to calculate N fluxes follow the ones of the framework in

Yang et al. [2021]. The land-use dependent protection coefficient h [Van Meter et al.,

2017] determines the amount of external N input that contributes to the protected

SON (SON(p)), and the residual contributes to the active SON (SON(a)).

Mineralization and denitrification are described as first-order processes. Based on the

results of Wang et al. [2023], the effect of wetness is considered in mineralization,

288 using:

289
$$MINE_a = k_a \cdot f(temp) \cdot f(wetness) \cdot SON_a$$
 (1)

290
$$MINE_p = k_p \cdot f(temp) \cdot f(wetness) \cdot SON_p$$
 (2)

$$291 DENI_S = \lambda_S \cdot SIN (3)$$

$$292 DENI_g = \lambda_g \cdot DIN (4)$$

where $MINE_a$, $MINE_p$ (kg ha⁻¹ day⁻¹) are the mineralization rates for active SON and protected SON, respectively. $DENI_s$ and $DENI_g$ (kg ha⁻¹ day⁻¹) are the denitrification rates for SIN and DIN, respectively. k_a , k_p , and λ (day⁻¹) are coefficients for the three first-order processes. f(temp) and f(wetness) are factors representing the constraints by soil temperature and wetness [Lindström et al., 2010; Wang et al., 2023], respectively. Plant uptake rate UPT follows the equation used in the HYPE model [Lindström et al., 2010]:

$$300 \quad UPT = min (UPT_P, 0.8 \cdot SIN) \tag{5}$$

301
$$UPT_P = p1/p3 \cdot (\frac{p_1-p_2}{p_2}) \cdot e^{-(DNO-p_4)/p_3}/(1 + (\frac{p_1-p_2}{p_2}) \cdot e^{-(DNO-p_4)/p_3})^2$$
 (6)

where UPT and UPT_P (kg ha⁻¹ day⁻¹) are the actual and potential uptake rates, respectively. The logistic plant growth function is considered in the equation of potential uptake rates. DNO is the day number within a year. p1, p2, p3 are three parameters depending on the type of plants, whose units are (kg ha⁻¹), (kg ha⁻¹), and (day), respectively. p4 is the day number of the sowing date. The leaching rate adopts a first-order process considering soil saturation and groundwater velocity, using:

$$308 \quad LEA = k_l \cdot f_w \cdot f_q \cdot SIN \tag{7}$$

$$309 f_w = \frac{S - S_r}{1 - S_r} (8)$$

$$310 f_q = MIN(\frac{q}{q_{ref}}, 1) (9)$$

where LEA is the leaching flux of SIN from the N source zone to the groundwater, k_l is a leaching coefficient (day-1), f_w and f_q are two factors representing the constraints of soil saturation and groundwater velocity to the leaching process, respectively. S is the soil saturation, and S_r is the residual saturation. q (m day-1) is the groundwater Darcy flow rate, q_{ref} (m day-1) is a reference Darcy flow rate. This formulation of LEA is modified from the one used in Van Meter et al. [2017].

In these hydrogeochemical processes, a portion of N is retained in the catchment as the biogeochemical legacy in soil or the hydrological legacy in groundwater or permanently leaves catchments by denitrification, which does not degrade the water quality of the catchment during a certain period. Therefore, the N retention is used to quantify a catchment's capacity to prevent nitrogen from entering surface water bodies during a certain period [Wang et al., 2023], which is the fraction of the N retained in the catchment and consumed via denitrification to the total external N input, calculated using [Ehrhardt et al., 2021]:

Retention =
$$1 - \frac{N_{\text{out}}}{N_{\text{in}}} = 1 - \frac{\int_{t_1}^{t_2} N_{\text{outlet}}}{\int_{t_1}^{t_2} N_{\text{input}}}$$
 (103)

where the N_{outlet} is the N mass leaving the catchment through the outlet during the time period $(t_1 - t_2)$.

Due to the lack of spatiotemporal variation information of the external N input, its value was fixed at 180 kg ha⁻¹ year⁻¹ according to Nguyen et al. [2021], where the N

balance was simulated in the upper Selke catchment covering the Schäfertal catchment. The protection coefficient h was selected as 0.3 according to the values reported in Van Meter et al. [2017]. p4 as the sowing date of plant growth activities was set to 63 days (early March) [Yang et al., 2018]. The DIN was transported in the coupled surface water-groundwater system, with longitudinal and transverse dispersion coefficients of 8 and 0.8 m, respectively. Other parameters relative to N dynamics were calibrated by PEST in empirical ranges. The measured CQ at the gauge station and the N surplus of 48.8 kg N ha⁻¹ year⁻¹ were used as the target variables. The calibration period spans from March 2001 to August 2003, during which successive C_Q data was were obtained. The CPU time was ~2 h for a single iteration. The N source zone serves as a boundary condition at the top of the aquifer for simulating DIN transport in the groundwater. The bedrock is treated as impermeable for water and nitrate. The catchment outlet is the only boundary allowing the exit of nitrate from the catchment. In order to minimize the influence of the initial conditions, a preliminary transport simulation (together with the flow simulation) was performed with zero loads in the SON and SIN pools and zero DIN concentration in the catchment, such that a quasi-steady state for the SON and SIN pools can be reached at the end of the preliminary simulation. The resulting data (N loads and concentrations) were used as initial conditions for the actual simulations.

330

331

332

333

334

335

336

337

338

339

340

341

342

343

344

345

346

347

3.3 Stochastic rainfall generator

349

350

351

352

353

354

355

356

357

358

359

360

361

362

363

364

365

366

367

368

In order to investigate the effect of rainfall variability on N dynamics, rainfall time series with different climatic characteristics were generated by a stochastic rainfall generator. The stochastic rainfall generator is a stochastic model of rainfall time series originally created to investigate the timescales of flood frequency response to rainfall, incorporating any combinations of storm, within-storm as well as between-storm, and seasonal variabilities of rainfall intensity [Robinson and Sivapalan, 1997]. It can output rainfall series representing different rainfall patterns under climate change. The equations can be found in Section S1 of the Supporting Information. We adopted the source code in Python v2.7 of the rainfall generator from Wilusz et al. [2017]. The stochastic model derives monthly average storm durations and inter-storm periods from seasonal parameters: averages (γ_s, δ_s) , amplitudes $(\alpha_{\gamma}, \alpha_{\delta})$, and phases $(\tau_{\gamma}\ ,\ \tau_{\delta}).\ a_1^1\sim a_1^4,\ b_1^1\sim b_1^4,\ a_2$ and b_2 are the parameters characterizing the dependence of average rainfall intensity on storm duration for the first season (Jan-Mar), the second season (Apr-June), the third season (Jul-Sep), and the fourth season (Oct-Dec). In addition, there is an isolated parameter P_{drizzle} in the source code, the probability of drizzle events. In the model, storms with precipitation smaller than 4_mm are drizzle events, while storms with precipitation greater than 4_mm can be identified as synoptic frontal events.

Rainfall time series representing different climate conditions were generated

369 following these steps below:

- 370 (i) To represent contrasting hydroclimatic conditions, Tthree representative
 371 years were selected from the 1997–2022 record (mean 607.9 mm; range
 372 408.2–916.3 mm)historical meteorological data, which are:—the wet year
 373 (2007, P = 916.3 mm), the normal year (2008, P = 588.7 mm), and the dry
 374 year (2018, P = 444.1 mm);
- 375 (ii) For each of the representative years, a set of parameters was determined so 376 that the generated rainfall time series can fit the actual rainfall data of this 377 year best. This inverse process was conducted using PEST;
- The three sets of best-fit parameters (Table 1) were used again to generate
 100 stochastic realizations (rainfall time series), for the wet, normal and dry
 year, respectively. These realizations may deviate from the actual rainfall
 data in terms of daily rainfall values, still being statistically identical with the
 rainfall pattern of the representative years.

Table 1. Three parameter sets of the rainfall generator for the wet, normal and dry year, respectively.

Parameter	Wet Year (2007)	Normal Year (2008)	Dry Year (2018)	Adjustable range	Note	
P(mm)	916.3	588.7	444.1	(400,1000)	Annual precipitation	
$P_{drizzle}$	0.137	0.146	0.140	(0.01, 0.99)	Probability of drizzle events	
Monthly mean storm duration γ						
$\gamma_s(\mathrm{day})$	2.546	2.177	2.071	(0.1, 10)	Seasonally averaged storm duration	
$\alpha_{\gamma}(\mathrm{day})$	1.764	0.820	0.550	(-2.2, 2.2)	Amplitude of seasonal storm shift	
$ au_{\gamma}(\mathrm{day})$	105.760	100.297	100.474	/	Phase of seasonal storm shifts	
Monthly mean inter-storm period δ						
$\delta_s(\mathrm{day})$	7.988	7.424	7.535	(0.1, 10)	Seasonally averaged inter-storm period	
$\alpha_{\delta}(\mathrm{day})$	2.457	2.962	2.946	(-8, 8)	Amplitude of seasonal inter-storm shift	
$\tau_{\delta}(\mathrm{day})$	120.665	124.044	124.161	/	Phase of seasonal inter-storm shifts	
Expected storm intensity $E[i t_r]$						
$(a_1,b_1)^1$	(0.875, 2.349)	(0.934, 1.802)	(0.909, 1.598)	(0.1, 5)	Coefficient 1 and 2 of the first season (Jan-Mar)	
$(a_1,b_1)^2$	(1.015, 0.661)	(0.894, 0.538)	(0.857, 0.456)	(0.1, 5)	Coefficient 1 and 2 of the second season (Apr-Jun)	
$(a_1,b_1)^3$	(0.917, 1.121)	(0.968, 0.845)	(0.947, 0.752)	(0.1, 5)	Coefficient 1 and 2 of the third season (Jul-Sep)	
$(a_1, b_1)^4$	(1.666, 1.556)	(1.348, 1.341)	(1.392, 1.263)	(0.1, 5)	Coefficient 1 and 2 of the fourth season (Oct-Dec)	
expected storm variability $CV^2[i t_r]$						
(a_2, b_2)	(0.658, 0.961)	(0.617, 1.057)	(0.632, 1.025)	(0.1, 5)	Coefficient 1 and 2	

3.4 Simulation scenarios

387

388

389

390

391

392

393

394

395

396

397

398

399

400

401

402

403

404

405

406

3.4.1 Inter-annual rainfall variability

Wet Year (WY), Normal Year (NY), and Dry Year (DY) (Table 1) were set as the simulation scenarios. In addition, a fourth scenario consistent with the Dry Year but coupled with reduced plant uptake was considered as Extreme Dry Year (EDY). This EDY scenario was used to account for the extreme drought occurring in 2018 that caused vegetation to die back and impacted N dynamics to some extent [Winter et al., 2023]. In the EDY scenario, the plant uptake was assumed to decrease down to 36% of the original value used in the DY scenario, according to the classification and the occurrence period of the drought [Liu et al., 2010]. To isolate the causal effects of rainfall variability on N dynamics, the time-invariant fertilization rate was used across all scenarios. For each of the scenarios, the water flow and N transport model were conducted 100 times by substituting the rainfall data during the simulation period with the generated 100 stochastic rainfall time series (Figure S1, Supporting Information). Average annual N loads and fluxes in each scenario were calculated to ensure that they were not controlled by a single realization and were statistically meaningful. Additionally, we simulated the fluctuations of CQ in each scenario with time over three years. Finally, the average annual N loads, fluxes, and C_Q as well as the variation of CQ were cross-compared and analyzed to elucidate the effect of inter-annual rainfall variability on N dynamics.

3.4.2 Intra-annual rainfall variability

407

408

409

410

411

412

413

414

415

416

417

418

419

420

421

422

423

424

425

426

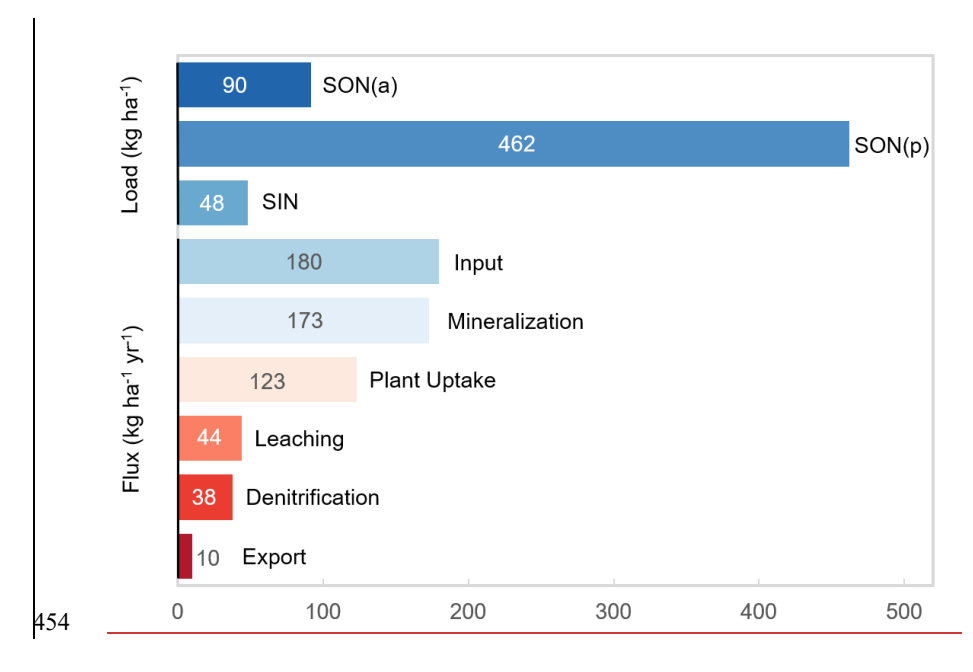
In order to explore the effect of intra-annual rainfall variability on N dynamics, the simple linear regression analyses were performed between the parameters of the stochastic rainfall-rainfall-generator parameters and each of the simulated annual N loads, fluxes, as well as and Co were conducted, in which the parameters of NY served as a reference. The seasonal averages of storm duration and inter-storm period (γ_s and δ_s), the amplitudes of the seasonal variations in storm duration and inter-storm period $(\alpha_{\gamma}$ and $\alpha_{\delta})$, the average rainfall intensity of four seasons $(E_1 \sim E_4)$ and squared coefficient of variation of the average rainfall intensity (CV2), as well as the probability of drizzle events (P_{drizzle}), were selected as the experimental parameters. $E_1 \sim E_4$ and CV^2 can be approximately calculated by equation S5 and S6, using relative parameters and seasonally averaged storm duration (γ_s). In total, 10 parameters (Table 1) were subjected to the assessment of their effect on N dynamics. For each of the experimental parameters, the rainfall generator generated 100 rainfall time series randomly, whose annual precipitation amounts are within the historical range, with this experimental parameter varying randomly within the adjustable range but other parameters being fixed to the best-fit values for the NY scenario. The ranges of the experimental parameters used in the linear regression analyses are listed in Table 1. Finally, the response of the annual N loads, fluxes and CQ to different rainfall parameters can be analyzed.

4 Results

427

428 The calibrated N transport model showed good performance in fitting the in-stream 429 nitrate concentration (Figure 4a), with a Nash-Sutcliffe efficiency (NSE) of 0.79. The modeled N surplus of 51.87 kg ha⁻¹ yr⁻¹ is comparable to the measured value of 48.8 430 kg ha⁻¹ yr⁻¹. The calibrated best-fit values for the transport parameters are listed in 431 Table S1 (see Supporting Information). 432 433 Figure 3 illustrates the 14-year N mass balance simulated by the calibrated N 434 transport model in the entire catchment. In the soil source zone, the total N consisted 435 of SON (552 kg ha⁻¹, including SON(a) of 90 kg ha⁻¹ and SON(p) of 462 kg ha⁻¹) and SIN (48 kg ha⁻¹). The load of SON accounts for 92% of the total N, which 436 corresponds to the research result that the organic N fraction is greater than 90% 437 438 [Stevenson-, 1995]. As for N transformation, the mineralization rate of 173 kg ha⁻¹ yr⁻¹ is within the range (14-187 kg ha⁻¹ yr⁻¹) reported by Heumann et al. [2011] for study 439 440 sites located in Germany. 71% of the SIN was absorbed by plants at a rate of 123 kg 441 ha-1 yr-1, which is very close to the value (around 120 kg ha-1 yr-1) suggested in Nguyen et al. [2021] for the same area. The denitrification flux of 38 kg ha⁻¹ yr⁻¹ (4 kg 442 ha⁻¹ yr⁻¹ in the soil source zone, 34 kg ha⁻¹ yr⁻¹ in the groundwater) is within the range 443 (8-51 kg ha⁻¹ yr⁻¹) investigated for 336 agricultural areas around the world by Hofstra 444 and Bouwman [2005]. The SIN entered the groundwater zone at a rate of 44 kg ha-1 445 yr⁻¹, which is within the range (15-60 kg N ha⁻¹ yr⁻¹) reported in Nguyen et al. [2021]. 446

Approximately 23% of the leachate of SIN was exported to the stream, where the rest of the leachate (77%) was removed by denitrification. The export and denitrification fluxes are comparable to the values of 39% and 61% reported in Nguyen et al. [2021]. Based on measured groundwater chemistry data from nearby catchments and multiple estimates of denitrification potential that have been proved and reported [Hannappel et al., 2018], we conclude that the simulated transformation and transport of N are acceptable.



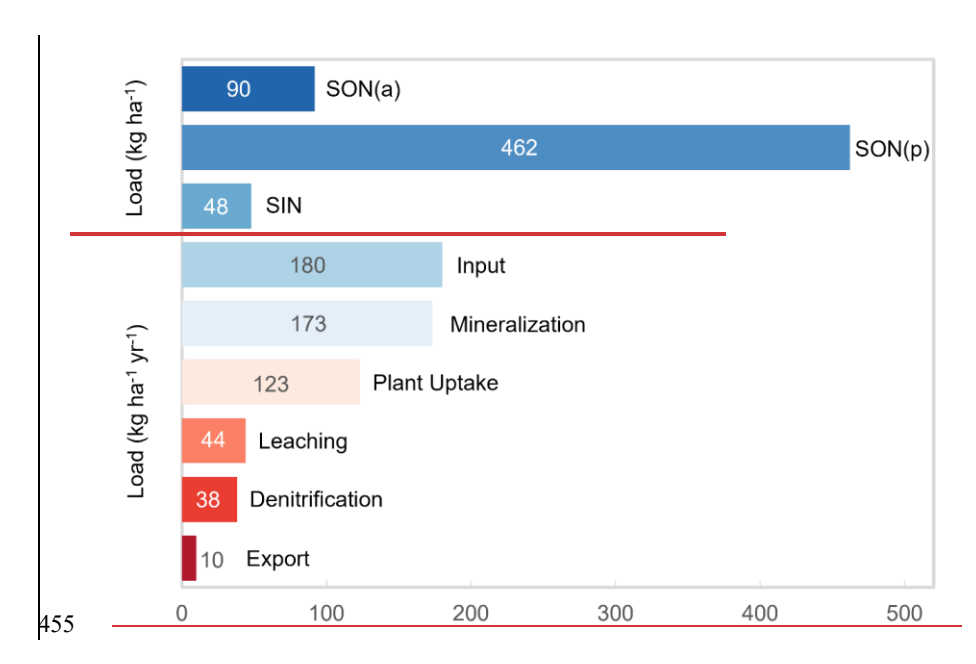


Figure 3. The simulated 14-year N mass balance in the entire catchment.

4.1 Effect of Inter-annual rainfall variability

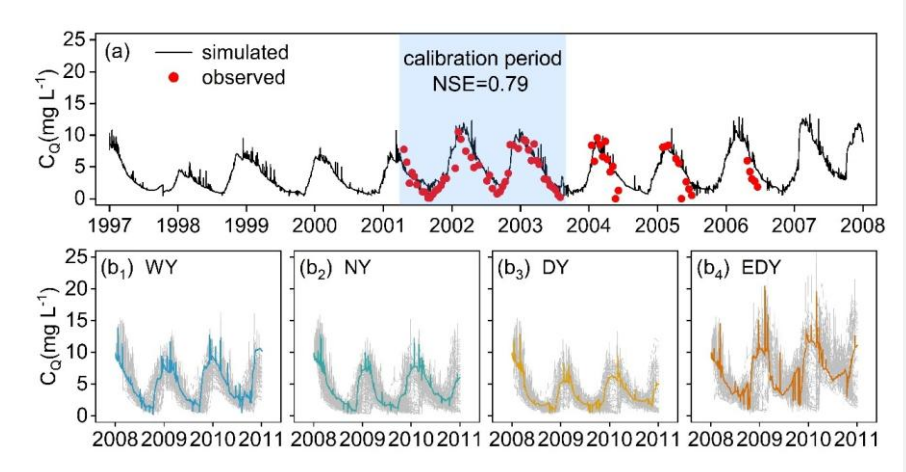


Figure 4. The fluctuations of simulated in-stream nitrate concentration (C_Q) under (a) the historical rainfall (1997-2007) and the scenarios of (b_1) WY, (b_2) NY, (b_3) DY, and (b_4) EDY (2008-2010). The grey areas are formed by the realizations of each scenario.

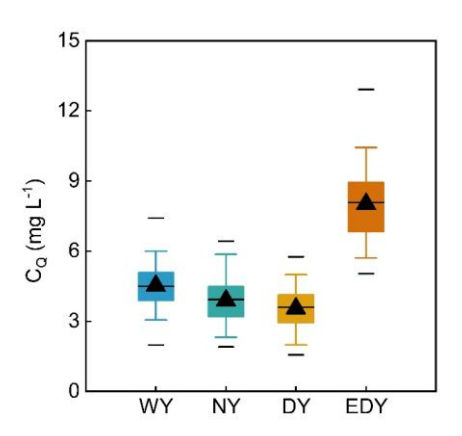


Figure 5. The simulated annual in-stream nitrate concentration (C_Q) for scenarios WY, NY, DY, and EDY. The whisker represents the concentration ranges-ranging from the 5th to 95th percentiles, with the triangles indicating the median and the lines marking the maximum, average, and minimum of the data set from top to bottom. The same notation is used as below.

The variations of C_Q in these scenarios are shown in Figure $4b_1 \sim 4b_4$. The range of C_Q generally decreases when the rainfall pattern transforms-shifts from WY, via NY, to DY, but the range of EDY is wider than that of WY. Figure 5 shows the range of the simulated annual in-stream nitrate concentration for the four scenarios. WY produced higher C_Q , with the median concentration reaching nearly 5 mg L^{-1} . The concentrations generally decreases when the rainfall pattern transforms from WY, via NY, to DY. However, when vegetation dieback occurred, most concentration values in the EDY scenario were far higher than those of WY. As shown in the results, the median concentration of EDY reached 8 mg L^{-1} . The soil organic nitrogen (SON(a) and SON(p)) loads increase when the rainfall pattern shifts from WY, via NY, to DY/EDY (Figure 6a and 6b). The SON loads in DY and EDY were identical because SONthe transformation—of SON is independent of sont subject to vegetation state.

There were no remarkable differences in soil inorganic nitrogen (SIN) load among WY, NY, and DY (Figure 6c). However, the SIN load in EDY was the highest among the four scenarios.

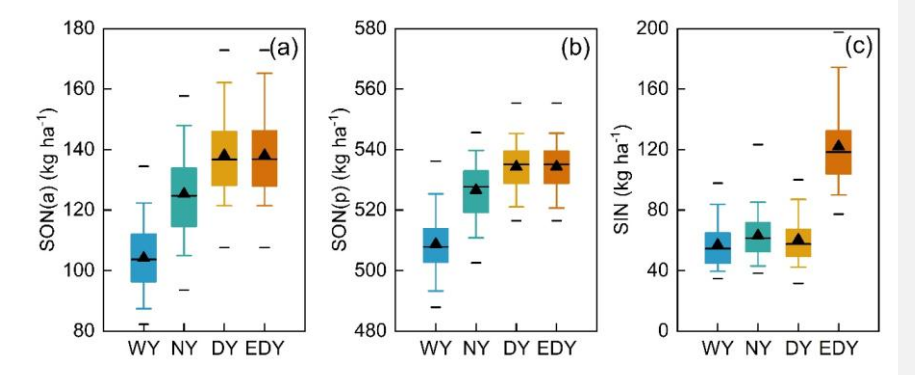


Figure 6. The simulated loads of (a) active soil organic nitrogen (SON(a)), (b) protected soil organic nitrogen (SON(p)), and (c) soil inorganic nitrogen (SIN) for scenarios WY, NY, DY, and EDY.

The highest and the lowest average mineralization levels were produced in WY and DY, respectively (Figure 7a). DY and EDY had have identical mineralization fluxes. Note that the fluxes of plant uptake, denitrification (in soil and groundwater), and leaching are negative values representing sink terms for the SIN pool (Figure 7b, 7c and 7d). These fluxes decrease when the rainfall pattern transforms from WY, via NY, to DY, due to decreasing soil moisture. In EDY, vegetation dieback resulted in Because of the the lowest level in plant uptakeaccumulated SIN load (Figure 6c) that resulted from the lowest level of plant uptake. Although the soil moisture content in EDY was low, denitrification and leaching fluxes in EDY with low annual precipitation were are still even larger than those of WY. The N export flux to the

stream generally follows the same trends as leaching, with relatively higher fluxes occurring in WY and EDY and lower fluxes in NY and DY (Figure 7e). Based on these results, it can be preliminarily concluded that annual precipitation and vegetation state critically influence N transformation and transport.

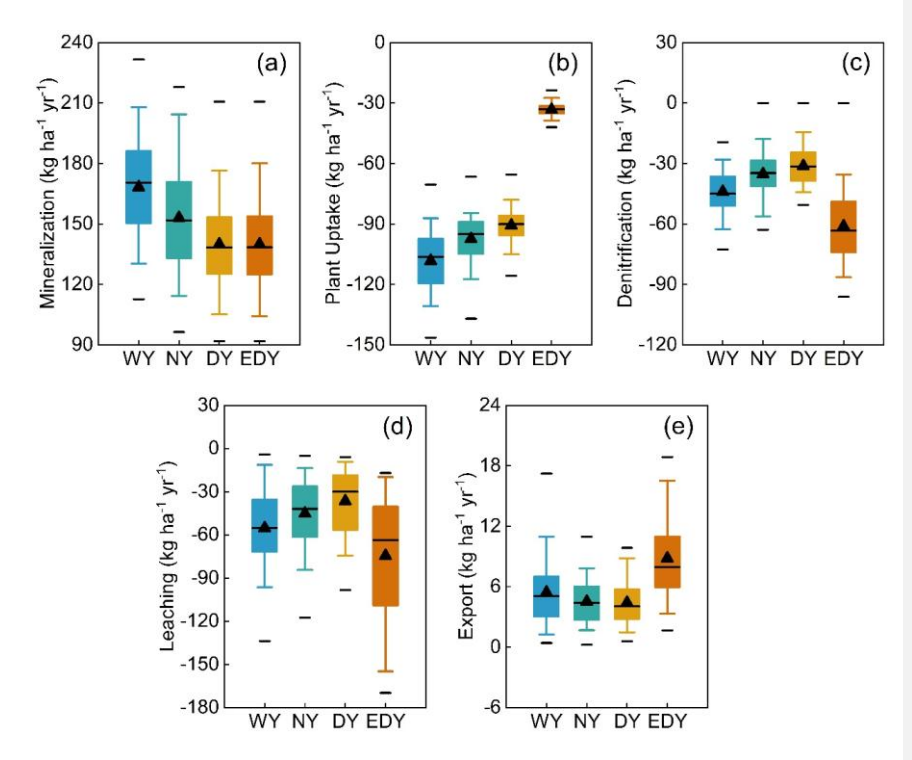


Figure 7. The simulated fluxes of (a) mineralization, (b) plant uptake, (c) denitrification (in soil and groundwater), (d) leaching, and (e) N export for scenarios WY, NY, DY, and EDY.

4.2 Effect of Intra-annual rainfall variability

The determination coefficients (R^2) of the linear regressions between the rainfall-generator parameters and the C_Q , N loads, and fluxes are illustrated in Figure 8a. Larger R^2 values can be observed for the amplitudes of the seasonal variations in

the storm duration and inter-storm period (α_{γ} and α_{δ}), the average rainfall intensity of the third season (E₃) as well as the probability of drizzle events (P_{drizzle}). These parameters are the four most important parameters (Figure 8b) that influence N dynamics, and are subject to further discussion.

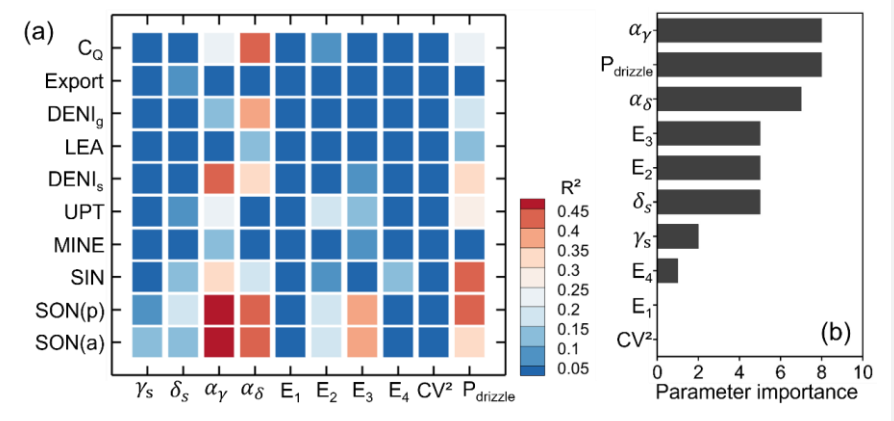


Figure 8. (a) The determination coefficients (R^2) of the linear regressions between the parameters of the rainfall generator and in-stream nitrate concentration (C_Q) , N loads, and fluxes. (b) The importance of the parameters influencing the N dynamics.

Storm duration

The parameter α_{γ} determines how the monthly average storm duration is distributed over the course of a year (Figure 9a). Generally, larger α_{γ} values represent that storms with longer duration are more likely to occur in mid-year when ET is high and the inter-storm duration is longer (yellow zone, Figure 9e). This pattern not only influences the drying and rewetting cycles in summer, but also supplies more water during this period, thereby leading to an overall wet year (e.g., year 2007, α_{γ} =1.764). A decrease in α_{γ} causes storms with longer durations to shift towards the

524 beginning/end of the year, when ET is low and the inter-storm duration is shorter 525 (blue zone, Figure 9e), so that the year becomes drier (e.g., year 2018, α_{γ} =0.55). 526 Results suggest that the storm duration distribution during a year significantly affects 527 N transformation and transport. Lower SON loads (Figure 9a: k=-28.04, p<0.05) and 528 higher SIN loads (Figure 9b; k=13.31, p<0.05) occurred when longer-duration storms 529 concentrate in mid-year. This is because wetter catchment conditions promote the 530 mineralization of SON into SIN, especially during warm periods when mineralization 531 is primarily constrained by soil moisture rather than temperature. The wetter 532 conditions associated with larger α_{ν} values increased the leaching flux of SIN from 533 soil to groundwater (Figure 9c; k=-4.77, $p \ge 0.05$), which elevated the average C_Q 534 (Figure 9d; k=0.7, p<0.05). When shorter-duration storms dominate mid-year, N 535 transformation and transport were inhibited.

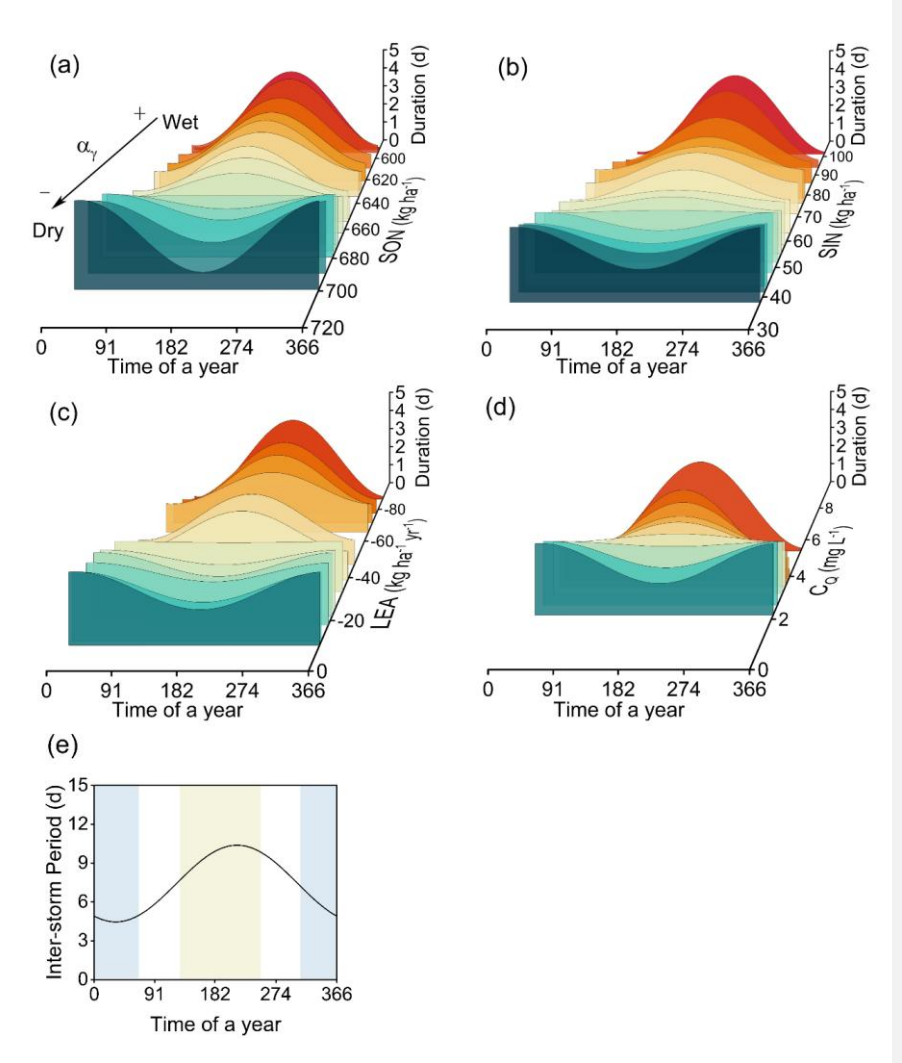


Figure 9. The effect of varying monthly average storm duration distributions over the course of a year on (a) SON load, (b) SIN load, (c) leaching flux (LEA), and (d) in-stream nitrate concentration (C_Q). (e) The monthly average inter-storm period distribution over the course of a year (α_δ is kept constant when α_γ varies). As α_γ values decrease, longer-durations storms shift gradually from the period with high ET and longer inter-storm periods (yellow zone) to the period with low ET and shorter inter-storm periods (blue zone).

Inter-storm period

 α_δ regulates the variation in monthly average inter-storm periods throughout the

course of a year (Figure 10a). Larger α_{δ} values cause longer inter-storm periods to cluster primarily in mid-year, coinciding with longer storm durations (blue zone, Figure 10e), while shorter inter-storm periods concentrate at the beginning/end of the year, associated with shorter storm durations (yellow zone, Figure 10e). This forms a "wet-dry-wet" climate pattern that promoted SON accumulation (Figure 10a; k=3.39, p<0.05) but reduced SIN load (Figure 10b; k=-1.34, p<0.05), leaching flux (Figure 10c; k=1.73, p<0.05), and C_Q (Figure 10d; k=-0.18, p<0.05). Conversely, decreasing α_{δ} redistributes longer inter-storm periods to the year's boundaries and shorter inter-storm periods to mid-year, thereby forming a "dry-wet-dry" climate pattern over a year. It resulted in a lower SON load and a higher SIN load, as mid-year warmth and moisture promoted the transformation and transport of SON accumulated in the previous season. Consequently, leaching flux and C_Q significantly increased.

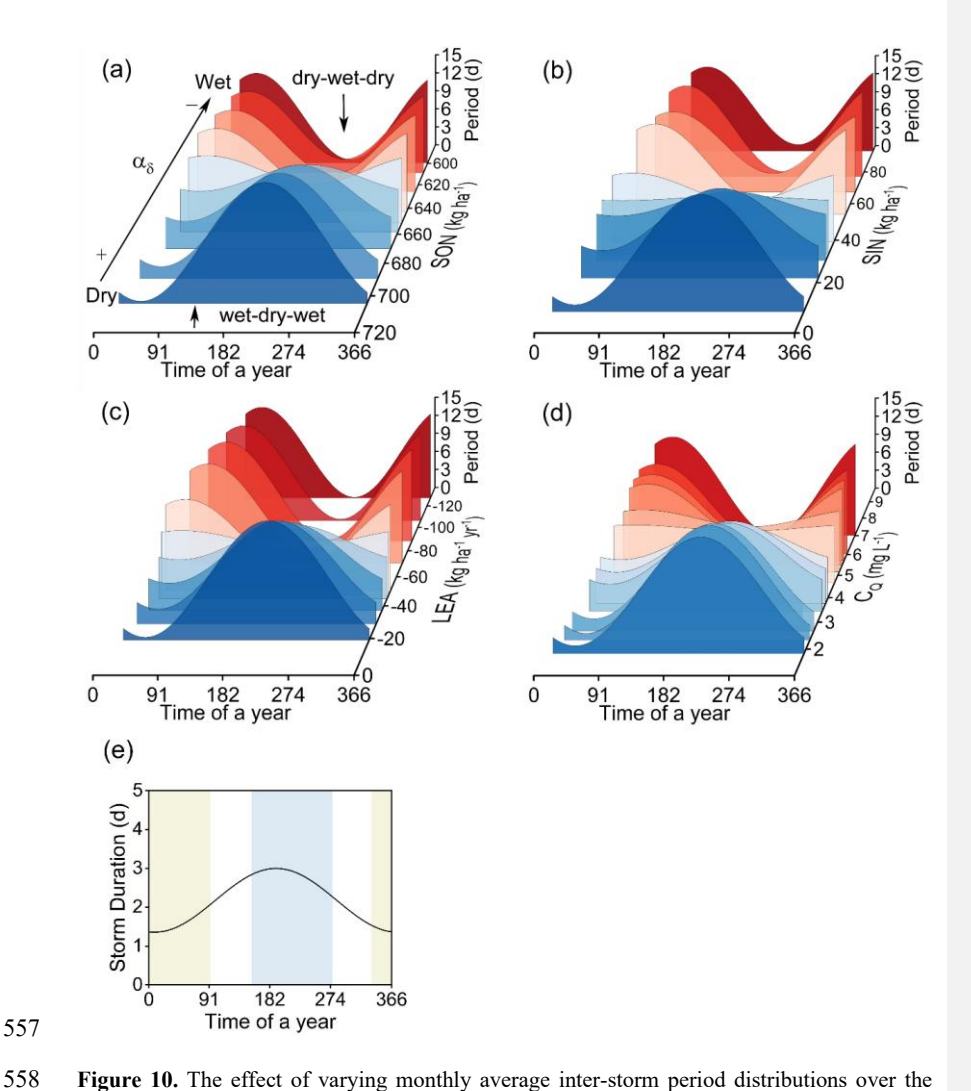


Figure 10. The effect of varying monthly average inter-storm period distributions over the course of a year on (a) SON load, (b) SIN load, (c) leaching flux (LEA), and (d) in-stream nitrate concentration (C_Q). (e) The monthly average storm duration distribution over the course of a year (α_γ is kept constant when α_δ varies). As α_δ values decrease, longer-periods inter-storms shift gradually from the period with longer storm durations (blue zone) to the period with shorter storm durations (yellow zone).

Average Storm Intensity

Figure 11 shows the responses of N loads, fluxes, and in-stream nitrate concentration

(C_Q) to seasonal average rainfall intensity (E₁-E₄). Fundamentally, increased rainfall intensity creates more humid conditions that intensify biogeochemical processes (e.g., mineralization, plant uptake). Based on determination coefficients (R²), linear regression slopes (k), and the significance, E2 and E3 generally exert stronger effects on N loads and fluxes than E1 and E4. Because mineralization that is the only source of SIN-remained unconstrained by temperature during the warm seasons (Figure 11b4 and 11c₄). Elevated E₂/E₃ enhanced the transformation of SON(a) (Figure 11b₁ and 11c₁) and SON(p) (Figure 11b₂ and 11c₂), whose loads significantly reduced decreased. Although SIN load theoretically should increase with rainfall intensity, as the only SON sink, it decreased in the second season (Figure 11b₃) due to substantially increased plant uptake (Figure 11b₅). Warmer temperatures and enhanced moisture during the growing season promoted vigorous nutrient absorption by vegetation (Figure 11b₅ and 11c₅). In addition, soil denitrification rose-increased markedly during the third season as average rainfall intensity increased (Figure 11c₆), which is was due to favorable microbial conditions-and-elevated SIN loads. In the fourth season, soil denitrification decreased slightly with increasing average rainfall intensity (Figure 11d₆), which was attributed to low temperatures and decreased SIN loads (Figure 11d₃). In warm periods, enhanced average rainfall intensity increased actual evapotranspiration (ET) (Figure S2b₁ and S2c₁), which correspondingly should reduce recharge and discharge. The linear relationships between seasonal average rainfall intensity and each of recharge, Q, N export, and Co are weak, with low R2 and

566

567

568

569

570

571

572

573

574

575

576

577

578

579

580

581

582

583

584

585

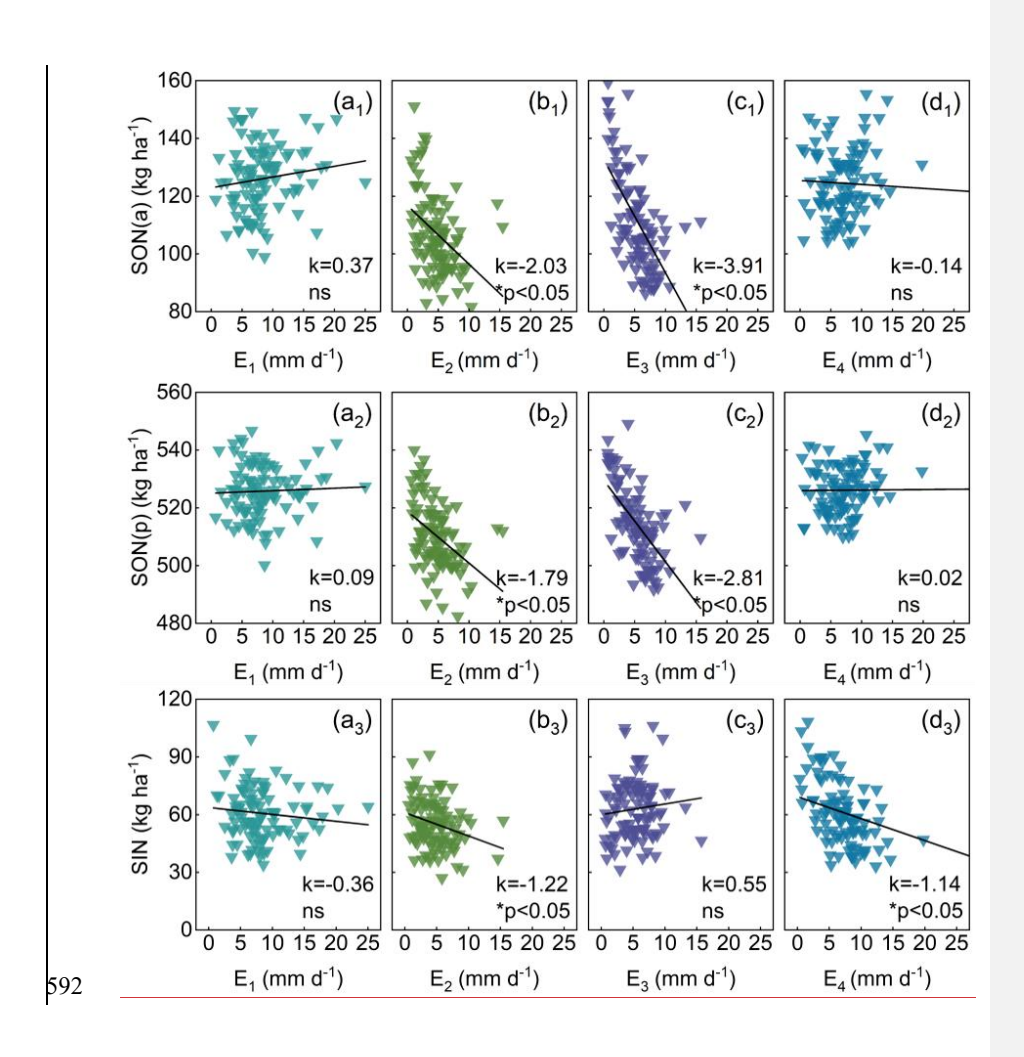
586

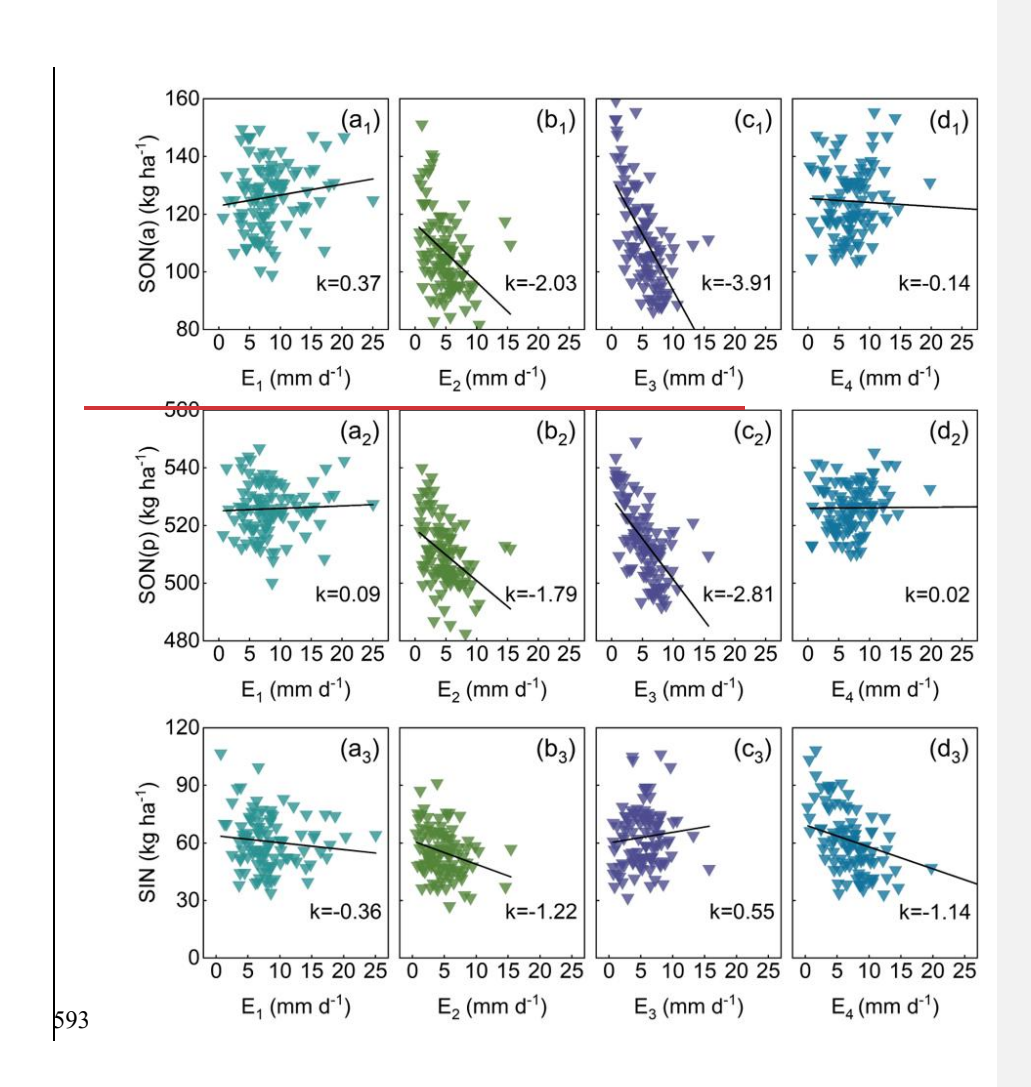
设置了格式: 上标

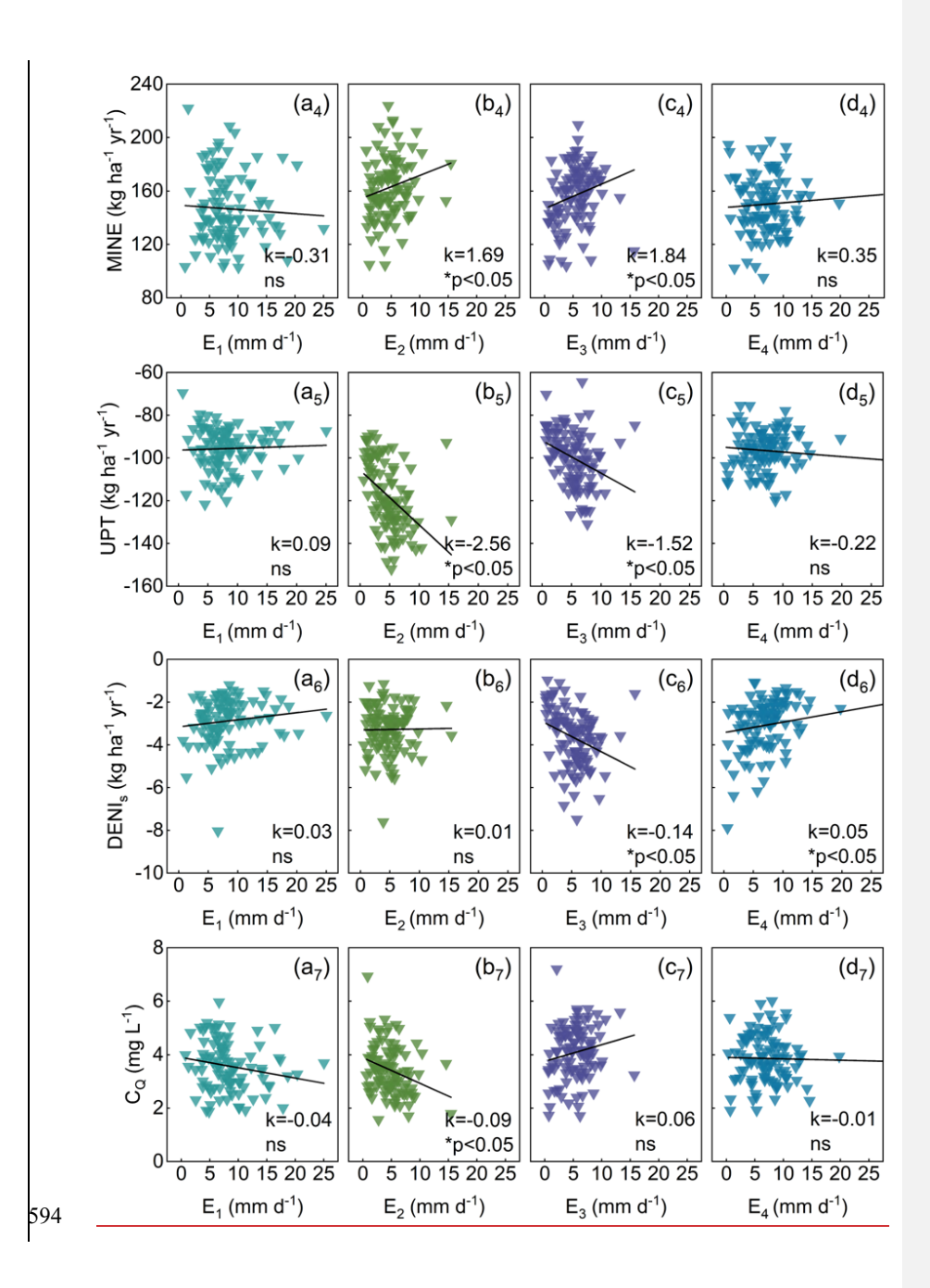
设置了格式:下标

1	
587	$small\ slope\ (k)\ values.\ Although\ several\ regressions\ reach\ statistical\ significance\ (p \leq$
588	0.05), their effects are minor (Figure 11b ₇ , S2a ₂ and S2d ₄). However, both recharge
589	and discharge increased during the second season (Figure S2b2 and S2b3). Export flux
590	and CQ-reduced slightly in the second season (Figure S2b4-and 11b7) but elevated in
591	the third season (Figure S2e4 and 11e2), mirroring SIN load trends.

设置了格式: 非上标/ 下标







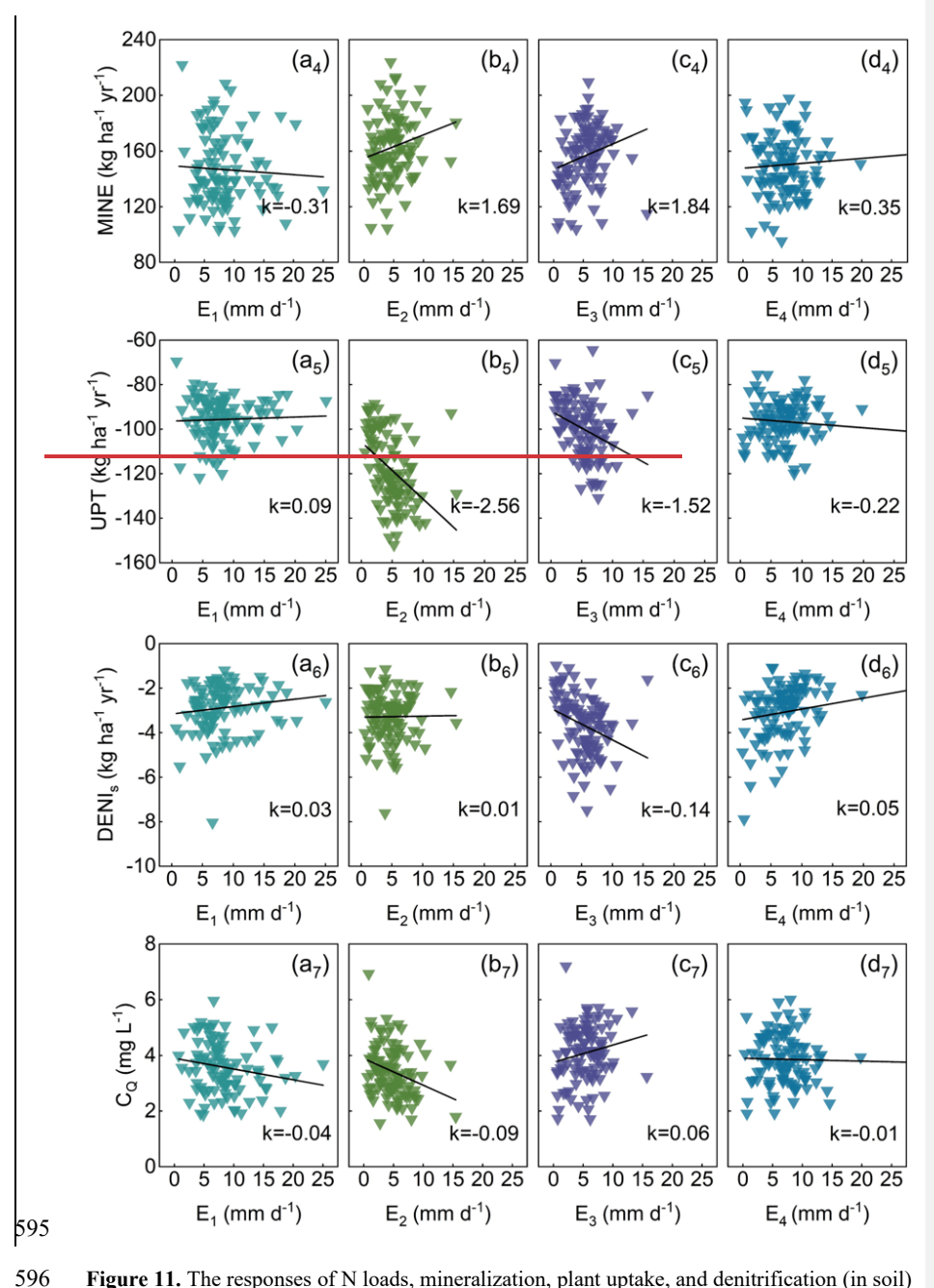


Figure 11. The responses of N loads, mineralization, plant uptake, and denitrification (in soil) fluxes, as well as in-stream nitrate concentration (C_Q) to the average rainfall intensity of the four seasons (E_1 - E_4). The sign and magnitude of the slopes (k) in these linear relationships

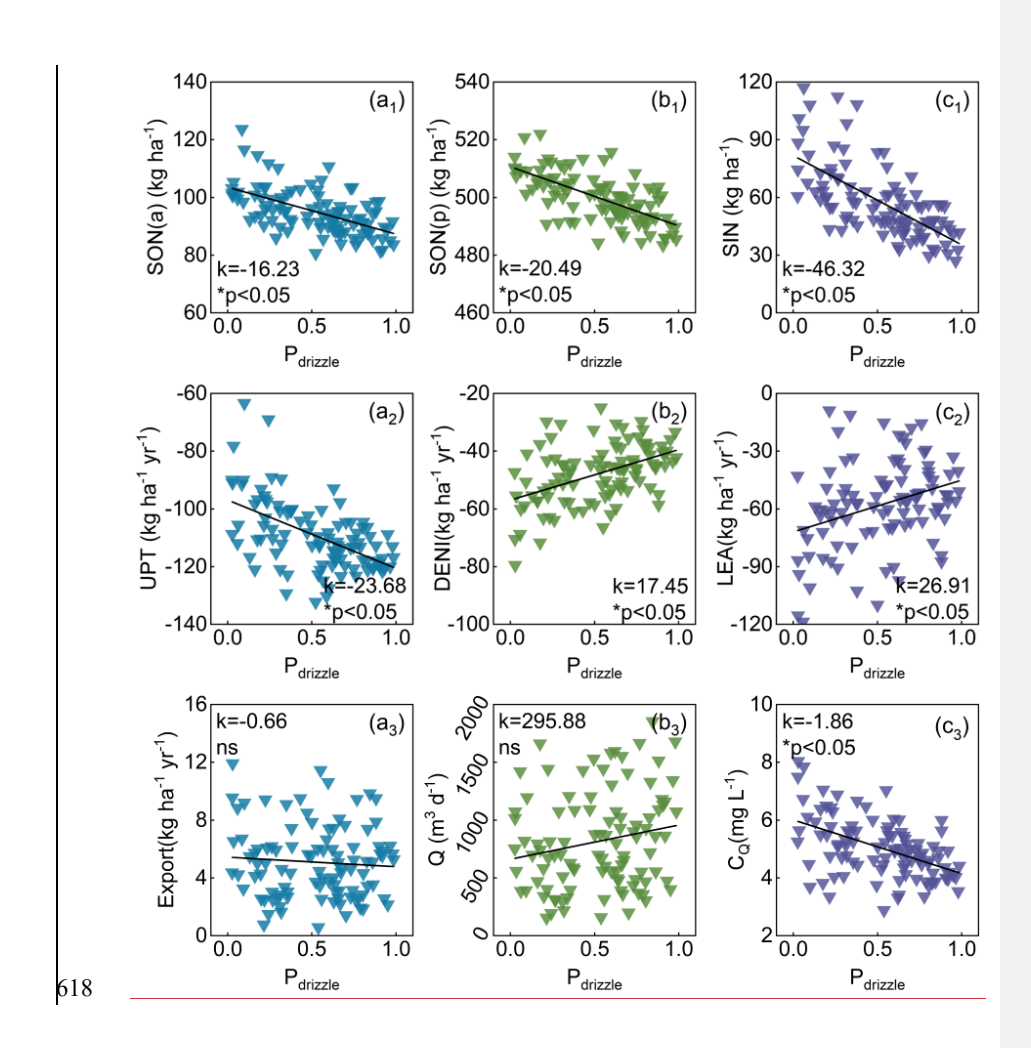
denote the direction and the-intensity of the response of N dynamics to the variations in average rainfall intensity, respectively. Asterisks indicate the significance of the regression slopes (p \leq 0.05); ns denotes non-significant relationships (p \geq 0.05).

Probability of drizzle event

Figure 12 illustrates the responses of N loads, fluxes, discharge (Q), and in-stream nitrate concentration (C_Q) to the probability of drizzle events (P_{drizzle}). P_{drizzle} characterizes the pattern of precipitation intensity over the course of a year. A low P_{drizzle} value indicates a predominance of moderately intense rainfall evenly distributed throughout the year, resulting in consistently humid conditions (e.g., year 2007, P_{drizzle}=0.137). Conversely, a high P_{drizzle} value represents the a situation with high-frequency drizzle and low-frequency extreme precipitation, forming drought-flood extremes. With the increase of P_{drizzle} (climate transition from consistently humid conditions to extreme drought-flood patterns), SON load decreased due to the enhanced transformation (Figure 12a₁ and 12b₁). Elevated plant uptake (Figure 12a₂) resulted in reduced SIN load decreased (Figure 12c₁) due to the elevated plant uptake (Figure 12a₂). Denitrification and leaching fluxes were reduced (Figure 12b₂ and 12c₂), while C_Q declined with increasing P_{drizzle} (Figure 12c₃). The linear relationships between P_{drizzle} and N export and between P_{drizzle} and C_Q are

设置了格式:字体: 五号

not significant (Figure 12a₃ and 12b₃; $p \ge 0.05$).



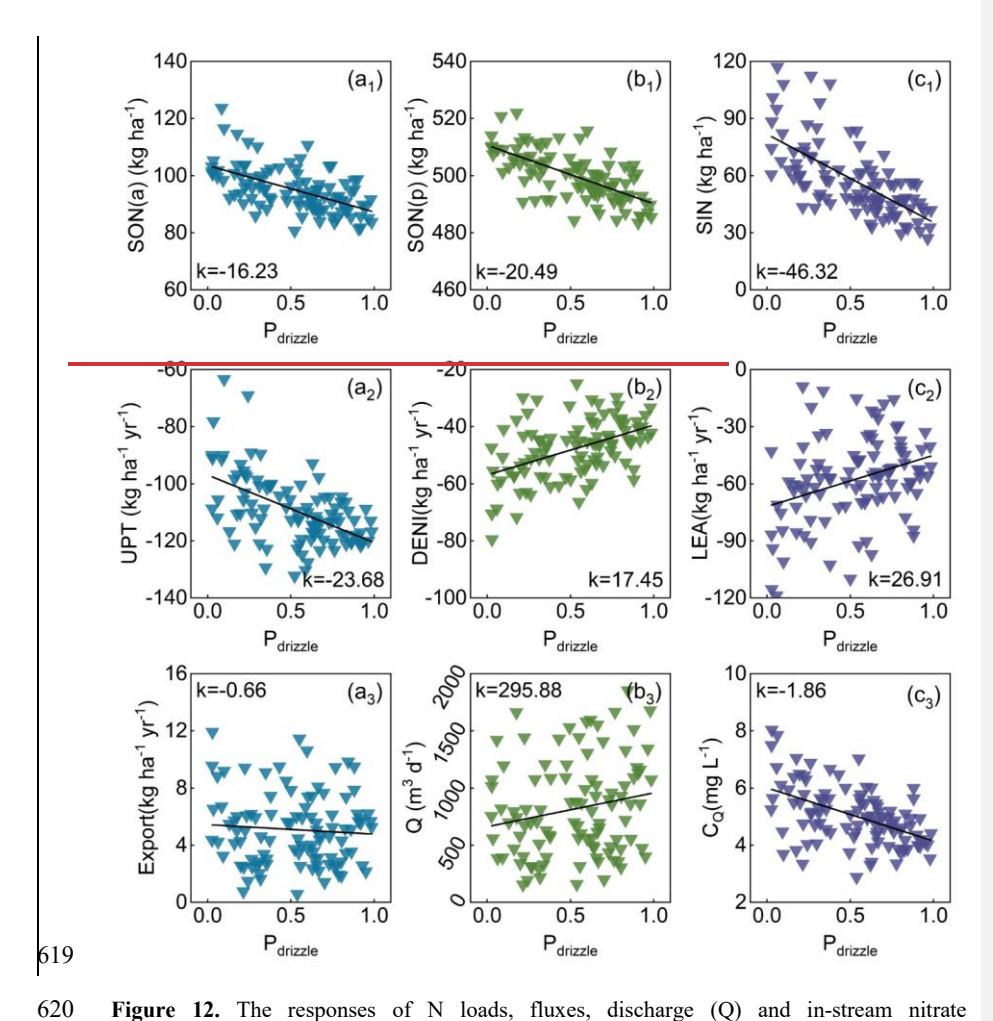


Figure 12. The responses of N loads, fluxes, discharge (Q) and in-stream nitrate concentration (C_Q) to the probability of drizzle events ($P_{drizzle}$). The sign and magnitude of the slopes (k) in these linear relationships denote the direction and the intensity of the response of N dynamics to the probability of drizzle events ($P_{drizzle}$) the variations in average rainfall intensity, respectively. Asterisks indicate the significance of the regression slopes ($p \le 0.05$); ns denotes non-significant relationships ($p \ge 0.05$).

5 Discussion

5.1 N transformation and transport upgrade in wet years

The comparison of CQ, N loads, and fluxes across four scenarios (WY, NY, DY, and

EDY) reveals the effect of inter-annual rainfall variability on N transformation and transport, as well as water quality. Mineralization, the crucial process of the transformation from SON to SIN, exhibits strong soil moisture dependence. Consequently, the highest average mineralization rates in the WY scenario promoted N transformation through plant uptake, denitrification, and leaching. In contrast, low mineralization in the DY scenario led to SON accumulation, thereby restraining overall N dynamics. Additionally, the transport of SIN relies on groundwater discharge and subsurface flow paths. Increased discharge from precipitation changes flushes more nitrogen into surface water bodies [Mitchell et al., 1996; Creed and Band, 1998] via fast shallow flow paths with short transit times (I-I cross section, Figure 1a) [Yang et al., 2018]. Consequently, N export and C_Q variations align with wetness changes among WY, NY, and DY. These results demonstrate that high annual precipitation enhances N transformation and transport, while low annual precipitation promotes catchment N retention. Our simulation results echo previous findings that N retention is influenced by changes in precipitation [Dumont et al., 2005; Howarth et al., 2006].

629

630

631

632

633

634

635

636

637

638

639

640

641

642

643

644

645

646

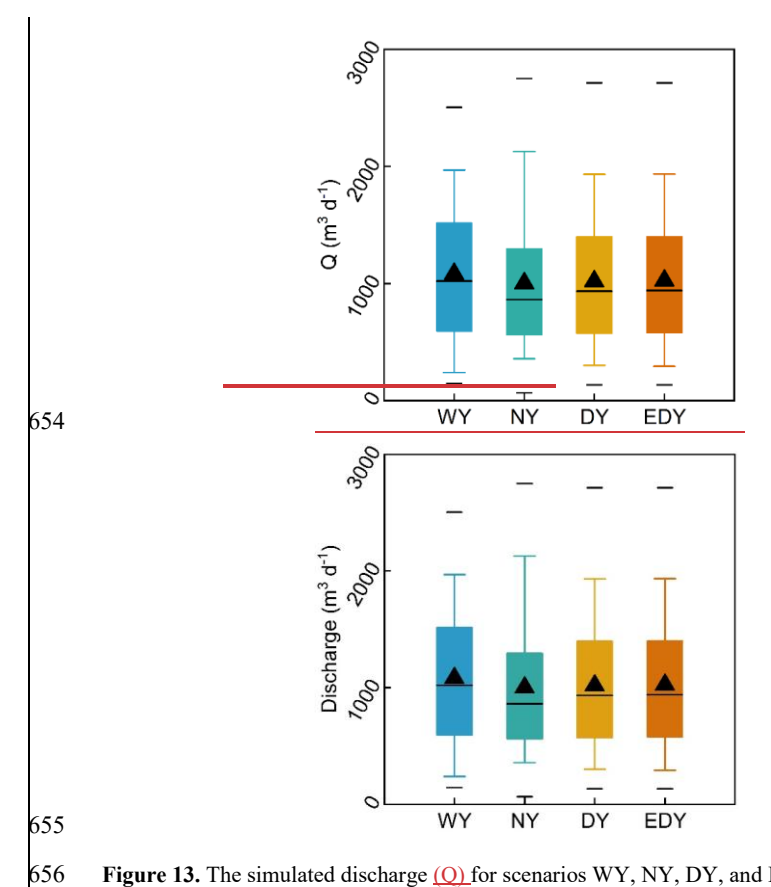
647

648

5.2 Stream water quality deteriorates during extreme droughts

SIN significantly accumulated in soil when the vegetation suffered from drought stress [RIVM, 2021; Winter et al., 2023]. This is because in general plant uptake is the major sink for SIN [Yang et al., 2021; Zhou et al., 2022; Wang et al., 2023]. Due to

the accumulation of SIN, denitrification and leaching in the EDY scenario were higher than those in the DY scenario. Thus, N export to the stream in the EDY scenario was higher than that in the DY scenario, even though their stream discharges wasere the same (Figure 13). This resulted in higher C_Q in the EDY scenario than that in the WY scenario.



649

650

651

652

653

657

658

659

Figure 13. The simulated discharge (O) for scenarios WY, NY, DY, and EDY.

During the 2018-2019 drought in central Europe, the observed peaks of in-stream nitrate concentration at a mesoscale catchment in central Germany were significantly higher than the previous concentration peaks (Figure 14). Based on the a data-driven analysis, Winter et al. [2023] indicated that nitrate loads in the 2018-2019 drought were up to 73% higher than the long-term average loads. They demonstrated that such increases were attributed to decreased plant uptake and subsequent flushing of accumulated nitrogen during the rewetting period. Our results confirm their findings that reduced plant uptake in extreme droughts causes C_{Q} to elevate significantly (Figure 4b₄) and the N retention capacity to decline. These results suggest that vegetation state plays a vital role in the increased risk of N pollution during extreme droughts.

660

661

662

663

664

665

666

667

668 669

671

672

673

674

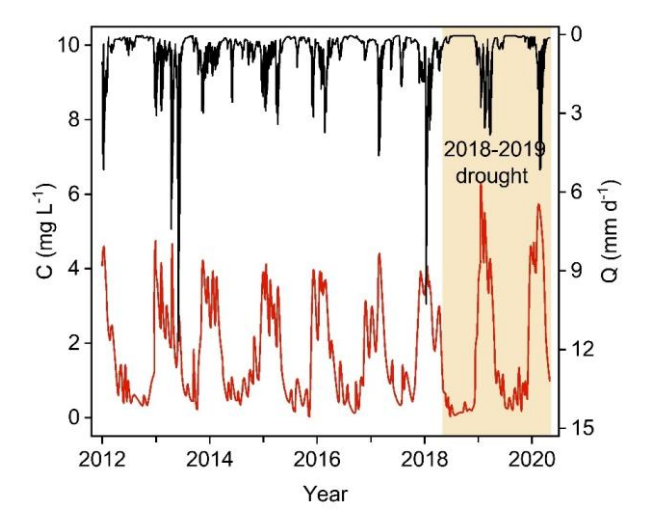


Figure 14. Measured daily averaged nitrate concentrations (C, red line) and discharge (Q, 670 black line) in the nearby Upper Selke catchment in central Germany [Winter et al., 2023]. The yellow area marks the 2018-2019 drought occurring across central Europe.

5.3 The distribution of storm durations controls the N loads

Our study indicates that the wet/dry conditions in mid-year are key to N transformation and transport throughout the whole year. The combination of longer storm durations and extended inter-storm periods in mid-year represents an aspect of extreme climate events where intense rainfall events alternate with droughts [Zhang et al., 2024]. Without temperature limitations, alternating longer storm durations and longer inter-storm periods increase the extensive SON transformation, which is consistent with the results of laboratory studies that mineralization increased increases after successive drying and rewetting cycles in soils [Cabrera, 1993]. It is concluded that drying-rewetting events induce the prominent changes in N dynamics [Fierer and Schimel, 2002]. However, the drier conditions induced by shortened storm durations and longer inter-storm periods in mid-year cause the accumulation of SON, which is consistent with the finding by Zhou et al. [2022] that the drought in the warm season contributed—contributes—to catchment nitrogen retention. Thus, storm duration distributions within a year can significantly affect N loads in a catchment.

5.4 The distribution of inter-storm periods changes stream water

688 quality

Different dry-wet patterns over the course of a year have an impact on N dynamics, particularly on in-stream nitrate concentration. In the "dry-wet-dry" pattern, accumulated SON from the dry season is transformed and transported during the subsequent wetting period, which leads to higher C_Q. During the 2018-2019 drought, accumulated N loads were flushed during the rewetting period and thereby caused elevated nitrate loads (Figure 14). In the "wet-dry-wet" pattern, humid conditions

with low temperatures $\frac{in-at}{in-at}$ the year's boundaries and warm droughts in mid-year both cause SON loads to accumulate throughout the entire year and C_Q to decrease. Zhou et al. [2022] attributed reduced C_Q to limited terrestrial export loads. In summary, inter-storm period distributions cause noticeable variations in water quality in terms of nitrate concentration.

5.5 Average rainfall intensity has only a small effect on stream water

quality

Wet conditions caused by high mean rainfall intensities enhance the transformation of SON to SIN [Knapp and Smith, 2001], when mineralization is not constrained by low temperatures (Equation 1 and 2). The potential plant uptake is subject to vegetation state (Equation 6), while the actual plant uptake is further limited by SIN load and soil moisture content (Equation 5) [Yang et al., 2022; Cramer et al., 2009]. Thus, high mean rainfall intensities promote plants absorption of SIN during active growth periods. Since plant uptake is the major sink of SIN, the responses of SIN load to mean rainfall intensity variations are jointly determined by mineralization and plant uptake, resulting in complex SIN load dynamics. SIN load controls denitrification in soil and leaching. However, denitrification is dependent on microbial conditions as well. However, IL eaching is a complex process—additionally influenced by soil saturation and groundwater velocity (Equation 3, 4, and 7). As a result, no significant linear relationship exists between mean rainfall intensity and leaching. Both soil

denitrification flux and N export flux (a component of leaching flux) vary with the average rainfall intensity, following SIN load patterns. It is noteworthy that high-intensity precipitation events with short durations and substantial surface runoff rarely propagate toreach the groundwater zonewater table, thereby exerting, minimally aeffects oning recharge, discharge, and nitrate N export (a component of leaching flux) (Figure S2, Supporting Information). Therefore, C_Q has shows weaker and non-significant responses into extreme precipitations.

5.6 Probability of drizzle event alters N dynamics

Extreme dry-wet patterns enhance the transformation of SON more effectively than continuously humid conditions, which echoes laboratory studies conducted by Cabrera [1993] that successive drying and rewetting cycles in soils can intensify mineralization. As the major sink, elevated plant uptake due to increased SIN load in turn reduced SIN load, which resulted in weaker denitrification and leaching. This is because denitrification and leaching are controlled by SIN load (Equation 3, 4, and 7). Following the same trends as leaching, CoN export flux slightly decreased. More discharge yielded in extreme dry wet patterns than in continuously humid conditions. The combination of increased discharge and slightly reduced N export led to a decrease in Co.—It follows that the probability of drizzle events prominently alters N dynamics.

On the whole, increased variations in precipitation can alter the transformation and transport of nitrogen [Kane et al., 2008]. The results of the present study can help in managing the water quality of agricultural catchments with prominent rainfall variability and protecting aquatic ecosystems during extreme rainfall events and droughts. For instance, a fertilization scheme for inter-storm periods can be formulated to avoid flushing during the rewetting periods after droughts. Also, increased fertilization in the growing season with humid conditions is not only conducive to vegetation absorption of nutrients, but also does not while not cause putting pressure on soil and water bodies.

5.7 Limitations and Outlook

The transport model preserves the main pathway for N-NO₃-leachate by simplifying the complexities of different N pools and transformations via mineralization, leaching, and denitrification within the soil zone. However, the external N input entering directly into inorganic N, the transformation from protected organic N to active organic N, and the loss of organic N via dissolution have not been included in the model, which may lead to miscalculations of nitrogen loads. As a complex biogeochemical process, denitrification is governed by various factors such as temperature, soil moisture content, and SIN load, rather than being a first-order decay process. Nonetheless, tThe current transport model does not account for spatial heterogeneity in denitrification. These simplifications may introduce uncertainties in

the simulated results. In addition, due to the lack of groundwater nitrate concentration data, the nitrate transport model was calibrated using only in-stream nitrate concentration data [Wang et al., 2023]. More nitrate concentration data in groundwater and rivers will contribute to establishing a more realistic nitrate transport model. The plant-soil process was not represented in the model. In the extreme dry scenario, plant death was not actually simulated under high temperature and low soil moisture content, but plants was were manually assigned a lower plant uptake potential. The plant growth stages were assumed to be constant. This is because the N uptake process was only mathematically described using the empirical formula (Equation 6) in the simplified N framework, rather than using a full plant-soil process. However, such simplification was proved to be effective in terms of reproducing reasonable N loads, fluxes and in-stream nitrate concentrations. Therefore, we think it is acceptable to identify the key effect of plant die-off (i.e., reduced N uptake potential) on stream water quality during extreme dry scenarios. In the future, the alteration of soil properties caused by rainfall variability should be studied. In the model, precipitation and the solute enter the subsurface domain with fixed soil porosity, ignoring the alteration of pores. Microorganisms and soil fauna are highly active, and soil organic and inorganic matter undergo continual biochemical

755

756

757

758

759

760

761

762

763

764

765

766

767

768

769

770

771

772

773

774

reactions Abundant microorganisms and animals engage in extensive activities, and

massive organic and inorganic matter undergoes biochemical reactions in soil pores, which all change the physical and chemical properties of porous media and thereby impact seepage. These biogeochemical processes are impacted by several factors, such as hydrometeorological conditions [Ondrasek et al., 2019]. For example, the activities of microorganisms and animals degrade under drying conditions, which is not beneficial for maintaining and improving soil structures. The severe deficit of soil moisture results in the disintegration of soil aggregates, and even compacted soil forming in the upper layer due to salt accumulationelusters, which ultimately reduces porosity. Additionally, cracked surface soil caused by extreme droughts is detrimental to plant growth and root development. Therefore, altered soil properties induced by complex and extreme climate patterns can substantially influence soil biogeochemical activities. The clarification of these mechanisms will be conducive to exploring the more realistic response of solute transport in groundwater to extreme rainfall events and droughts.

6 Conclusions

Within the context of climate change and the increasing occurrence of extreme rainfall events and droughts, the study pioneered the application of a stochastic rainfall generator (Robinson and Sivapalan, 1997) coupled with the flow and transport model to systematically investigate inter-annual and intra-annual rainfall variability effects on N dynamics in a small agricultural catchment located in Central Germany.

795 The principal findings are as follows:

801

802

803

804

808

809

810

- 196 (1) Higher annual precipitation enhances N transformation and transport, whereas
 lower annual precipitation is conducive to the N retention capacity. Nonetheless,

 198 *The retention capacity declines severely when vegetation suffers from drought
 199 stress. Vegetation plays a vital role in the response of N dynamics especially
 190 duringto extreme droughts.
 - (2) Wet/dry conditions determined by storm duration distributions within a year can significantly affect N loads in a catchment. Droughts can prompt the accumulation of SON, but a drying-wetting cycle can enhance extensive SON transformation in the warm season.
- 805 (3) Different dry-wet patterns formed by inter-storm period distributions during a year

 806 can cause noticeable variations in in-stream nitrate concentrations that

 807 prominently elevate during the rewetting period after a drought.
 - (4) Elevated mean rainfall intensity contributes to N transformation when mineralization is not constrained by low temperatures, and promotes plant absorption of SIN during the growing season. There is merely a small effect on stream water quality.
- 812 (5) The probability of drizzle events, characterizing the pattern of precipitation
 813 intensity within a year, prominently alters N dynamics. Extreme dry-wet patterns
 814 enhance SON transformation and plant uptake but inhibit denitrification and

816 Overall, the study clarifies the effect of rainfall variability on N dynamics in a small 817 agricultural catchment, which provides theoretical support for formulating fertilization strategies and protecting aquatic ecosystems in the context of climate 818 819 change. 820 Code availability. All data used in this study are listed in the supporting information 821 and uploaded separately to HydroShare [Wang, 2024]. 822 Author contributions. QW contributed to the conceptualization, methodology, 823 software, formal analysis, visualization, and writing (review and editing). JY 824 contributed to the conceptualization, methodology, formal analysis, and writing 825 (review and editing). IH contributed to the writing (review and editing). TX 826 contributed to the conceptualization and review and editing. CL contributed to the 827 methodology, and review and editing. 828 Competing interests. The contact author has declared that none of the authors has any 829 competing interests. 830 Disclaimer. Publisher' note: Copernicus Publications remains neutral with regard to 831 jurisdictional claims in published maps and institutional affiliations.

leaching more effectively than continuously humid conditions.

815

832

833

Acknowledgements. We thank Daniel C. Wilusz for the source code in Python v2.7 of

the rainfall generator [Wilusz et al., 2017] and Min Yan and Huiqiang Wu for

834	stimulating discussions. We thank the editorial board for handling our manuscript
835	especially two anonymous reviewers, whose constructive comments helped improve
836	the manuscript.
837	Financial support. This research was supported by the National Natural Science
838	Foundation of China, China (U2340212), the National Key Research and
839	Development Project, China (JY: 2024YFC3211600) and, the National Natura
840	Science Foundation of China, China (JY & CL: U2340212, TX: 42377046, CL
841	51879088), the Fundamental Research Funds for the Central Universities, China (JY
842	B250201002).5 Ingo Heidbüchel acknowledges the support from the German
843	Research Foundation - DFG, Germany (IH: 454619223). Teng Xu and Chunhui Lu
844	acknowledge the support from and the National Natural Science Foundation of China
845	(42377046, 51879088) and the Natural Science Foundation of Jiangsu Province
846	China (CL: BK20190023)

Reference

- Acreman, M. C.: A simple model of hourly rainfall for Farnborough, England, Hydrol. Sci. J.,
- 849 35, 119-148, 1990.
- 850 Altermann, M., Mautschke, J.: Ergebnisbericht über quartärgeologische bodenhydrologische
- 851 Untersuchungen im Gebiet des Schäfertals und Waldbachs bei Siptenfelde, VEB GFE Halle,
- 852 1970.

- 853 Altermann, M., Pretzschel, M., Mautschke, J., Erbe, C.: Zur Kennzeichnung der quartären
- Deckschichten im Unterharz, Petermanns Geografische Mitteilungen 2/77, 1977.
- 855 Altermann, M., Steininger, M.: Vom Bodenprofil zum Gebietswasserhaushalt
- Untersuchungen aus dem Unterharz, Mitteilungen der DBG, 74, 167-170, 1994.

- 857 Alvarez-Cobelas, M., Angeler, D.G., Sánchez-Carrillo, S.: Export of nitrogen from
- 858 catchments: a worldwide analysis, Environ. Pollut., 156 (2), 261-269
- 859 https://doi.org/10.1016/j.envpol.2008.02.016, 2008.
- 860 Amatya, I. M., Kansakar, B. R., Tare, V., & Fiksdal, L.: Impact of Temperature on Biological
- 861 Denitrification Process, J. Instit. Engineer., 7(1), 121–126
- 862 https://doi.org/10.3126/jie.v7i1.2070, 2009.
- Anis, M. R., & Rode, M.: Effect of climate change on overland flow generation: A case study
- 864 in central Germany, Hydrol. Proc., 29(11), 2478–2490, 2015.
- 865 Bach, M., Frede, H.-G.: Agricultural nitrogen, phosphorus and potassium balances in
- 866 Germany methodology and trends 1970 to 1995, Zeitschrift für Pflanzenernährung und
- 867 Bodenkunde, 161 (4), 385–393, https://doi.org/10.1002/jpln.1998.3581610406, 1998.
- 868 Bach, M., Godlinski, F., Greef, J.-M.: Handbuch Berechnung der Stickstoffbilanz für die
- Landwirtschaft in Deutschland, Jahre 1990–2008, 159, 2011.
- 870 Ballard, T.C., Sinha, E., Michalak, A.M.: Long-term changes in precipitation and temperature
- have already impacted nitrogen loading, Environ. Sci. Technol., 53 (9), 5080–5090, 2019.
- 872 Bauwe. A., Kahle. P., Tiemeyer. B., & Lennartz. B.: Hydrology is the key factor for nitrogen
- 873 export from tile-drained catchments under consistent land-management, Environ. Res. Lett.,
- 874 15 094050, https://doi.org/10.1088/1748-9326/aba580, 2020.
- 875 Borchardt, D.: Geoökologische Erkundung und hydrologische Analyse von
- 876 Kleineinzugsgebieten des unteren Mittelgebirgsbereichs, dargestellt am Beispiel von
- 877 Experimentalgebieten der oberen Selke/Harz, Petermanns Geografische Mitteilungen, 4/82,
- 878 1981.
- 879 Cabrera, M.: Modeling the flush of nitrogen mineralization caused by drying and rewetting
- 880 soils, Soil Sci. Soc. Am. J., 57: 63-66, 1993.
- 881 Chow, V. T., D. R. Maidment, and L. W. Mays.: Applied Hydrology, 572 pp., McGraw-Hill,
- 882 New York, 1988.
- 883 Cramer, M. D., Hawkins, H.-J., and Verboom, G. A.: The importance of nutritional regulation
- 884 of plant water flux, Oecologia, 161, 15–24, https://doi.org/10.1007/s00442-009-1364-3, 2009.
- 885 Delpla, I., Jung, A.-V., Baures, E., Clement, M., & Thomas, O.: Impacts of climate change on
- 886 surface water quality in relation to drinking water production, Environ. Int., 35(8), 1225–1233,
- 887 https://doi.org/10.1016/j.envint.2009.07.001, 2009.
- 888 Doherty, J. E., & Hunt, R. J.: Approaches to highly parameterized inversion-a guide to using
- pest for groundwater-model calibration (Tech. rep 2010-5211), Reston, VA: US Geological
- 890 Survey, 2010.

- 891 Creed IF, Band LE.: Export of nitrogen from catchments within a temperate forest: evidence
- 892 for a unifying mechanism regulated by variable source area dynamics, Water Resour. Res., 34:
- 893 3105-3120, 1998.
- Dumont, E. L., Harrison, J. A., Kroeze, C., Bakker, E. J., Seitzinger, S. P.: Global distribution
- and sources of dissolved inorganic nitrogen export to the coastal zone: results from a spatially
- 896 explicit, global model, Global Biogeochem. Cycles, 19: GB4S02, DOI
- 897 10.1029/2005GB002488, 2005.
- 898 Dupas, R., Musolff, A., Jawitz, J.W., Rao, P. S. C., Jäger, C. G., Fleckenstein, J. H., Rode, M.,
- 899 Borchardt, D.: Carbon and nutrient export regimes from headwater catchments to downstream
- 900 reaches, Biogeosciences, 14 (18), 4391–4407, https://doi.org/10.5194/bg- 14-4391-2017,
- 901 2017.
- 902 Fink, A. H., Brücher, T., Krüger, A., Leckebusch, G. C., Pinto, J. G., Ulbrich, U.: The 2003
- 903 European summer heatwaves and drought-synoptic diagnosis and impacts, Weather, 59, 209-
- 904 216, 2004.
- 905
- 906 Fierer, N., Schimel, J. P.: Effects of drying-rewetting frequency on soil carbon and nitrogen
- 907 transformations, Soil Biol. Biochem., 34:777-787, 2002.
- 908 Geris, J., Comtea, J. C., Franchib, F., Petrosc, A., Tirivarombob, S., Selepeng, A., Villholth,
- 909 K.: Surface water-groundwater interactions and local land use control water quality impacts
- 910 of extreme rainfall and flooding in a vulnerable semi-arid region of Sub-Saharan Africa, J.
- 911 Hydrol., S0022-1694(22)00409-7, https://doi.org/10.1016/j.jhydrol.2022.127834, 2022.
- 912 Graeff, T., Zehe, E., Reusser, D., Lück, E., Schröder, B., Wenk, G., John, H., Bronstert, A.:
- 913 Process identification through rejection of model structures in a mid-mountainous rural
- 914 catchment: Observations of rainfall-runoff response, geophysical conditions and model
- 915 inter-comparison, Hydrol. Proc., 23(5), 702–718, https://doi.org/10.1002/hyp.7171, 2009.
- 916 Haag, D., Kaupenjohann, M.: Landscape fate of nitrate fluxes and emissions in central Europe:
- a critical review of concepts, data, and models for transport and retention, Agric. Ecosyst.
- 918 Environ., 86 (1), 1–21, 2001.
- 919 Hanel, M., Rakovec, O., Markonis, Y., Maca, P., Samaniego, L., Kysely, J., & Kumar, R.:
- 920 Revisiting the recent European droughts from a long-term perspective, Sci. Rep., 8, 1–11,
- 921 2018.
- 922 Hannappel, S., Köpp, C., Bach, T.: Charakterisierung des Nitratabbauvermögens der
- 923 Grundwasserleiter in Sachsen-Anhalt, Grundwasser Zeitschrift der Fachsektion
- 924 Characterization of the denitrification potential of aquifers in Saxony-Anhalt, Hydrogeologie,
- 925 23 (4), 311–321, 2018.

- 926 Hari, V., Rakovec, O., Markonis, Y., Hanel, M., & Kumar, R.: Increased future occurrences
- 927 of the exceptional 2018-2019 Central European drought under global warming, Sci. Rep.,
- 928 10(1), 1–10, https://doi.org/10.1038/s41598-020-688729, 2020.
- 929 Hesse, C., Krysanova, V.: Modeling climate and management change impacts on water
- 930 quality and in-stream processes in the Elbe River Basin, Water, 8 (2), 40, 2016.
- 931 Heumann, S., Ringe, H., Bottcher, J.: Field-specific simulations of net N mineralization based
- 932 on digitally available soil and weather data. I. Temperature and soil water dependency of the
- 933 rate coefficients, Nutr. Cycl. Agroecosyst., 91 (2), 219-234,
- 934 https://doi.org/10.1007/s10705-011-9457-x, 2011.
- 935 Hofstra, N., Bouwman, A.F.: Denitrification in agricultural soils: summarizing published data
- 936 and estimating global annual rates, Nutr. Cycl. Agroecosyst., 72 (3), 267-278.
- 937 https://doi.org/10.1007/s10705-005-3109-y, 2005.
- 938 Howarth, R. W., Swaney, D. P., Boyer, E. W., Marino, R., Jaworski, N., Goodale, C.: The
- 939 influence of climate on average nitrogen export from large watersheds in the Northeastern
- 940 United States, Biogeochemistry, 79: 163-186, 2006.
- 941 Huff, F. A.: Time distribution of rainfall in heavy storms, Water Resour. Res., 3, 1007-1018,
- 942 1967.
- Ionita, M., Tallaksen, L. M., Kingston, D. G., Stagge, J. H., Laaha, G., Van Lanen, H. A. J.,
- 944 Scholz, P., Chelcea, S. M., Haslinger, K.: The European 2015 drought from a climatological
- 945 perspective, Hydrol. Earth Syst. Sci., 21, 1397–1419, 2017.
- 946 IPCC.: Climate change 2007: the physical science basis, vol 1009, Cambridge University
- 947 Press, Cambridge, 2007.
- Kane, E., Betts, E., Burgin, A. J., Clilverd, H., Crenshaw, C. L., Fellman, J., Myers-Smith, I.,
- 949 O'donnell, J., Sobota, D. J., Van Verseveld, W. J.: Precipitation control over inorganic
- 950 nitrogen import-export budgets across watersheds: a synthesis of longterm ecological
- 951 research, Ecohydrology, 1, 105–117, 2008.
- 952 Knapp, A. K., Smith, M. D.: Variation among biomes in temporal dynamics of aboveground
- 953 primary production, Science, 291: 481-484, 2001.
- 954 Laaha, G., Gauster, T., Tallaksen, L. M., Vidal, J.-P., Stahl, K., Prudhomme, C.,
- 955 Heudorfer, B., Vlnas, R., Ionita, M., Van Lanen, H. A. J., Adler, M., Caillouet, L., Delus, C.,
- 956 Fendekova, M., Gailliez, S., Hannaford, J., Kingston, D., Van Loon, A. F., Mediero, L.,
- 957 Osuch, M., Romanowicz, R., Sauquet, E., Stagge, J. H., & Wong, W. K.: The European 2015
- 958 drought from a hydrological perspective, Hydrol. Earth Syst. Sci., 21, 3001-3024,
- 959 https://doi.org/10.5194/hess-21-3001-2017, 2017.

- 960 Leitner, S., Dirnböck, T., Kobler, J., Zechmeister-Boltenstern, S.: Legacy effects of drought
- 961 on nitrate leaching in a temperate mixed forest on karst, J. Environ. Manage., 262, 110338,
- 962 2020.
- 963 Lindström, G., Pers, C., Rosberg, J., Strömqvist, J., and Arheimer, B.: Development and
- 964 testing of the HYPE (Hydrological Predictions for the Environment) water quality model for
- 965 different spatial scales, Hydrol. Res., 41.3 4, 2010.
- 966 Liu, E., Mei, X., Gong, D., Yan, C., Zhuang, Y.: Effects of drought on N absorption and
- 967 utilization in winter wheat at different developmental stages, Chin. J. Plant Ecol., 34 (5): 555-
- 968 562, 2010.
- 969 Liu, X., He, B., Guo, L., Huang, L., & Chen, D.: Similarities and differences in the
- 970 mechanisms causing the European summer heatwaves in 2003, 2010, and 2018, Earth's
- 971 Future, 8(4): e2019EF001386, https://doi.org/10.1029/2019EF001386, 2020.
- 972 Min, S. K., Zhang, X., Zwiers, F. W., & Hegerl, G. C.: Human contribution to more-intense
- 973 precipitation extremes, Nature, 470, 378–381, 2011.
- 974 Mitchell, M. J., Driscoll, C. T., Kahl, J. S., Likens, G. E., Murdoch, P. S., Pardo, L. H.:
- 975 Climatic control of nitrate loss from forested watersheds in the northeast United States,
- 976 Environ. Sci. Technol., 30:2609-2612, 1996.
- 977 Mosley, L. M.: Drought impacts on the water quality of freshwater systems; review and
- 978 integration, Earth Sci. Rev., 140, 203–214, 2015.
- 979 Nguyen, T. V., Kumar, R., Lutz, S. R., Musolff, A., Yang, J., & Fleckenstein, J. H.: Modeling
- 980 nitrate export from a mesoscale catchment using storage selection functions, Water Resour.
- 981 Res., 56, e2020WR028490, 10.1029/2020WR028490, 2021.
- 982 Ondrasek, G., Begić, B. H., Zovko, M., Filipović, L., Meriño-Gergichevich, C., Savić, R.,
- 983 Rengel, Z.: Biogeochemistry of soil organic matter in agroecosystems & environmental
- 984 implications, Sci. Total Environ., 658, 1559-1573, ISSN 0048-9697
- 985 https://doi.org/10.1016/j.scitotenv.2018.12.243, 2019.
- 986 Orth, R., Vogel, M. M., Luterbacher, J., Pfister, C., & Seneviratne, S. I.: Did European
- temperatures in 1540 exceed present-day records, Environ. Res. Lett., 11, 1–10, 2016.
- 988 Otkin, J., Svoboda, M., Hunt, E. D., Ford, T. W., Anderson, M., Hain, C., & Basara, J. B.:
- 989 Flash droughts: A review and assessment of the challenges imposed by rapid onset droughts
- 990 in the United States, Bull. Amer. Meteor. Soc., 99, 911-919,
- 991 https://doi.org/10.1175/BAMS-D-17-0149.1, 2018.
- 992 Pall, P., Aina, T., Stone, D., Stott, P., Nozawa, T., Hillberts, A., Lohmann, D., Allen, M.:
- 993 Anthropogenic greenhouse gas contribution to flood risk in England and Wales in autumn
- 994 2000, Nature, 470, 382–385, 2011.

- 995 Pendergrass, A. G., Knutti, R., Lehner, F., Deser, C., & Sanderson, B. M.: Precipitation
- variability increases in a warmer climate, Sci. Rep., 7, 17966, 2017.
- 997 Robinson, J., & Sivapalan, M.: Temporal scales and hydrological regimes: Implications for
- 998 flood frequency scaling, Water Resour. Res., 33, 12, 2981-2999,
- 999 https://doi.org/10.1029/97WR01964, 1997.
- 1000 Schuldt, B., Buras, A., Arend, M., Vitasse, Y., Beierkuhnlein, C., Damm, A., Gharun, M.,
- 1001 Grams, T. E. E., Hauck, M., Hajek, P., Hartmann, H., Hiltbrunner, E., Hoch, G.,
- 1002 Holloway-Phillips, M., Körner, C., Larysch, E., Lübbe, T., Nelson, D. B., Rammig, A.,
- Rigling, A., Rose, L., Ruehr, N. K., Schumann, K., Weiser, F., Werner, C., Wohlgemuth, T.,
- 1004 Zang, C. S., & Kahmen, A.: A first assessment of the impact of the extreme 2018 summer
- 1005 drought on Central European forests, Basic Appl. Ecol., 45, 86-103
- 1006 https://doi.org/10.1016/j.baae.2020.04.003, 2020.
- 1007 Stahl, K., Kohn, I., Blauhut, V., Urquijo, J., De Stefano, L., Acácio, V., Dias, S., Stagge, J. H.,
- 1008 Tallaksen, L. M., Kampragou, E., Van Loon, A. F., Barker, L. J., Melsen, L. A., Bifulco, C.,
- 1009 Musolino, D., de Carli, A., Massarutto, A., Assimacopoulos, D., & Van Lanen, H. A. J.:
- 1010 Impacts of European drought events: insights from an international database of text-based
- 1011 reports, Nat. Hazards Earth Syst. Sci., 16, 801–819, doi:10.5194/nhess-16-8012016, 2016.
- 1012 Stevenson, F. J.: Humus chemistry: genesis, composition, reactions, Second Edition, Wiley. J
- 1013 Chem Educ., doi: 10.1021/ed072pA93.6, ISBN: 978-0-471-59474-1, 512 pp, 1995.
- 1014 Therrien, R., McLaren, Sudicky, R. E., & Panday, S.: Hydrogeosphere: A three-dimensional
- numerical model describing fully-integrated subsurface and surface flow and solute transport,
- 1016 Groundwater Simulations Group, Waterloo, ON: University of Waterloo, 2010.
- 1017 Thieken, A. H., Kienzler, S., Kreibich, H., Kuhlicke, C., Kunz, M., Mühr, B., Müller, M.,
- 1018 Otto, A., Petrow, T., Pisi, S., & Schröter, K.: Review of the flood risk management system in
- $1019 \quad \text{Germany} \quad \text{after} \quad \text{the} \quad \text{major} \quad \text{flood} \quad \text{in} \quad 2013, \quad \text{Ecol.} \quad \text{Soc.}, \quad 21(2)\text{:}51,$
- 1020 http://dx.doi.org/10.5751/ES-08547-210251, 2016.
- 1021 Trenberth, K. E.: Changes in precipitation with climate change, Clim. Res., 47, 123-138,
- 1022 2011.
- 1023 Ulbrich, U., Brücher, T., Fink, A., Leckebusch, G. C., Krüger, A., & Pinto, J. G.: The central
- European floods of August 2002: Part 1 Rainfall periods and flood development, Weather,
- 1025 58(10):371-377, DOI: 10.1256/wea.61.03A, 2003.
- 1026 Van Meter, K. J., Basu, N. B., Van Cappellen, P.: Two centuries of nitrogen dynamics:
- 1027 Legacy sources and sinks in the Mississippi and susquehanna river basins, Global
- 1028 Biogeochem. Cycles, 31 (1), 2–23., https://doi.org/10.1002/2016GB005498, 2017.
- 1029 Vitousek, P. M., Naylor, R., Crews, T., David, M. B., Drinkwater, L. E., Holland, E., Johnes,
- 1030 P. J., Katzenberger, J., Martinelli, L. A., Matson, P. A., Nziguheba, G., Ojima, D., Palm, C.

- 1031 A., Robertson, G. P., Sanchez, P. A., Townsend, A. R., Zhang, F. S.: Nutrient imbalances in
- agricultural development. Science, 324(5934), 1519–1520, 10.1126/science.1170261, 2009.
- 1033 Voit, P., & Heistermann, M.: A downward-counterfactual analysis of flash floods in Germany,
- 1034 Nat. Hazards Earth Syst. Sci., 24, 2147–2164, https://doi.org/10.5194/nhess-24-2147-2024,
- 1035 2024.
- 1036 Wang, Q.: DS2024-1WQ, HydroShare,
- 1037 <u>http://www.hydroshare.org/resource/1199c12ae64447bd87d5c005a11e984c</u>, 2024.
- 1038 Wang, Q., Yang, J., Heidbüchel, I., Yu, X., Lu, C.: Flow paths and wetness conditions explain
- spatiotemporal variation of nitrogen retention for a temperate, humid catchment, J. Hydrol.,
- 1040 625(2):130024, DOI: 10.1016/j.jhydrol.2023.130024, 2023.
- 1041 Watmough, S. A., Aherne, C. E. J., Dillon, P. J.: Climate Effects on Stream Nitrate
- 1042 Concentrations at 16 Forested Catchments in South Central Ontario, Environ. Sci. Technol.,
- 1043 38(8):2383-8, DOI: 10.1021/es0351261, 2004.
- Whitehead, P.G., Wilby, R. L., Battarbee, R. W., Kernan, M., Wade, A. J.: A review of the
- potential impacts of climate change on surface water quality, Hydrol. Sci. J., 54 (1), 101–123,
- 1046 2009.
- 1047 Williams, A. P., Seager, R., Abatzoglou, J. T., Cook, B. I., Smerdon, J. E., Cook, E. R.:
- 1048 Contribution of anthropogenic warming to California drought during 2012-2014, Geophys.
- 1049 Res. Lett., 42(16):6819-6828, DOI: 10.1002/2015GL064924, 2015.
- 1050 Wilusz, D. C., Harman, C. J., & Ball, W. P.: Sensitivity of catchment transit times to rainfall
- variability under present and future climates, Water Resour. Res., 53, 10,231-10,256,
- 1052 https://doi.org/10.1002/2017WR020894, 2017.
- Winter, C., Nguyen, T., Musolff, A., Lutz, S., Rode, M., Kumar, R., Fleckenstein, J.:
- 1054 Droughts can reduce the nitrogen retention capacity of catchments, Hydrol. Earth Syst. Sci.,
- 1055 27(1):303-318, https://doi.org/10.5194/hess-27-303-2023, 2023.
- 1056 Winter, C., Müller, S., Kattenborn, T., Stahl, K., Szillat, K., Weiler, M., Schnabel, F.: Forest
- 1057 dieback in drinking water protection areas a hidden threat to water quality, BioRxiv, doi:
- $1058 \qquad https://doi.org/10.1101/2024.08.07.606951, 2024. \\$
- 1059 Wollschläger, U., Attinger, S., Borchardt, D., Brauns, M., Cuntz, M., Dietrich, P.: The bode
- 1060 hydrological observatory: A platform for integrated, interdisciplinary hydro-ecological
- 1061 research within the Tereno Harz/central German lowland observatory, Environ. Earth Sci.,
- 1062 76(1), 29, https://doi.org/10.1007/s12665-016-6327-5, 2016.
- 1063 Yang, J., Graf, T., & Ptak, T.: Impact of climate change on freshwater resources in a
- 1064 heterogeneous coastal aquifer of Bremerhaven, Germany: A three-dimensional modeling
- 1065 study, J. Contam. Hydrol., 177, 107–121, 2015.

- 1066 Yang J., Heidbüchel, I., Musolff, A., Reinstorf, F., & Fleckenstein. J. H.: Exploring the
- dynamics of transit times and subsurface mixing in a small agricultural catchment, Water
- 1068 Resour. Res., 54, https://doi.org/10.1002/2017WR021896, 2018.
- 1069 Yang J., Heidbüchel, I., Musolff, A., Xie, Y., Lu, C., Fleckenstein. J. H.: Using nitrate as a
- tracer to constrain age selection preferences in catchments with strong seasonality, J. Hydrol.,
- 1071 603 (2021) 126889, https://doi.org/10.1016/j.jhydrol.2021.126889, 2021.
- 1072 Yang, X., Rode, M., Jomaa, S., Merbach, I., Tetzlaff, D., Soulsby, C., & Borchardt, D.:
- 1073 Functional multi-scale integration of agricultural nitrogen-budgets into catchment water
- 1074 quality modeling, Geophys. Res. Lett., 49, e2021GL096833,
- 1075 https://doi.org/10.1029/2021GL096833, 2022.
- 1076 Zhang, W., Furtado, K., Wu. P., Zhou, T., Chadwick, R., Marzin, C., Rostron, J., & Sexton,
- 1077 D.: Increasing precipitation variability on daily-to-multiyear time scales in a warmer world,
- 1078 Sci. Adv., 7, eabf8021, 2021.
- 1079 Zhang, W., Zhou, T., Wu, P.: Anthropogenic amplification of precipitation variability over
- 1080 the past century, Science, 385, 427–432,
- 1081 https://www.science.org/doi/10.1126/science.adp0212, 2024.
- 1082 Zhou, X., Jomaa, S., Yang, X., Merz, R., Wang, Y., Rode, M.: Exploring the relations
- 1083 between sequential droughts and stream nitrogen dynamics in central Germany through
- 1084 catchment-scale mechanistic modelling, J. Hydrol., 614 (2022) 128615
- 1085 <u>https://doi.org/10.1016/j.jhydrol.2022.128615</u>, 2022.
- 1086 Zwolsman, J. J. G., van Bokhoven, A. J.: Impact of summer droughts on water quality of the
- Rhine River a preview of climate change?, Water Sci. Technol., 56 (4), 45–55, 2007.

The effect of rainfall variability on Nitrogen

dynamics in a small agricultural catchment

- 3 Qiaoyu Wang^{1,3}, Jie Yang^{1,2}, Ingo Heidbüchel^{4,5}, Teng Xu^{1,3}, Chunhui Lu^{1,2}
- ⁴ The National Key Laboratory of Water Disaster Prevention, Hohai University, Nanjing,
- 5 China
- 6 ²College of Hydrology and Water Resources, Hohai University, Nanjing, China
- ³College of Water Conservancy and Hydropower Engineer, Hohai University, Nanjing,
- 8 China
- 9 ⁴UFZ Helmholtz-Centre for Environmental Research GmbH, Department of
- 10 Hydrogeology, Leipzig, Germany
- 11 ⁵Hochschule Koblenz, Koblenz, Germany
- 12 Correspondence to: Jie Yang (yangj@hhu.edu.cn); Chunhui Lu (clu@hhu.edu.cn)

Table S1. The parameters for the N source zone. The parameters were adjustable and calibrated
 (referring to *Yang et al.* [2022]).

Parameter	Process	Adjustable range	Reference	Value of best fit
k_a	Mineralization	0~0.7	Van Meter et al. [2017]	0.0111 day ⁻¹
k_p	Mineralization	0~0.7	Van Meter et al. [2017]	0.0008 day ⁻¹
<i>p</i> 1	Plant uptake	60~160	Van Meter et al. [2017]	160 kg·ha ⁻¹
<i>p</i> 2	Plant uptake	1~10		10 kg·ha ⁻¹
р3	Plant uptake	1~60		34 day
λ_s	Denitrification in soil	0~0.7	Nguyen et al. [2021]	0.0007 day ⁻¹
k_l	Leaching	1~1000		18.8888 day ⁻¹
q_{ref}	Leaching	1e ⁻⁴ ~1		0.01 m·day ⁻¹
λ	Denitrification in water	1e ⁵ ~1e ⁻¹	Nguyen et al. [2021]	0.0088 day-1

S1 Stochastic rainfall generator

16

Daily rainfall time series with specific climatic characteristics are generated by the stochastic rainfall generator in three steps [Robinson & Sivapalan, 1997]. First, determining a series of alternating storm durations t_r and inter-storm periods t_b over the simulation time. It is hypothesized that t_r and t_b are independent of each other and vary seasonally. Each t_r and t_b as random variables are sampled from the exponential (and shifted exponential) probability density functions (pdf) regarding monthly mean storm duration γ and mean inter-storm period δ , respectively:

24
$$f_{T_r}(t_r|\gamma) = \frac{1}{\gamma} exp\left(-\frac{t_r}{\gamma}\right) \quad t_r > 0$$
 (S1)

25
$$f_{T_b}(t_b|\delta) = \frac{1}{\delta - \varepsilon} exp\left(-\frac{t_b - \varepsilon}{\delta - \varepsilon}\right) \quad t_b > \varepsilon$$
 (S2)

- where the shift ε is the specified minimum dry period of 24 hours. Both γ and δ are
- 27 assumed as sinusoidally with time of year τ as follow:

28
$$\gamma = \gamma_s + \alpha_{\gamma} \sin\left\{\frac{2\pi}{\omega_h}(\tau - \tau_{\gamma})\right\}$$
 (S3)

29
$$\delta = \delta_s + \alpha_\delta \sin\left\{\frac{2\pi}{\omega_h}(\tau - \tau_\delta)\right\}$$
 (S4)

- 30 where γ_s and δ_s are the seasonally averaged storm duration and inter-storm period,
- 31 respectively. α_{γ} and α_{δ} are the amplitudes of the seasonal variations in γ and δ .
- 32 τ_{γ} and τ_{δ} are seasonal phase shifts of t_r and t_b . ω_h is the total number of time
- units in a year. If τ , τ_{γ} , and τ_{δ} are in days, ω_h is equal to 365 days. Regional
- 34 climates are determined by multiple factors, such as atmosphere, geography, hydrology,
- 35 and biology). As a result, τ_{γ} and τ_{δ} are definite and steady for a certain area.
- However, climate change may reflect in the variation of γ_s , δ_s , α_{γ} and α_{δ} , which

- 37 alters the average level of storm duration and inter-storm period and their distribution
- 38 during a year.
- 39 Second, determining the average rainfall intensity i of each storm. Average rainfall
- 40 intensity i is set as a random variable stochastically dependent on storm duration t_r ,
- which means that i and t_r follow the joint probability density function, $f_{I,T_r}(i,t_r|\gamma)$.
- In order to characterize the dependence between i and t_r , it is assumed that the
- 43 conditional statistics of $E[i|t_r]$ and $CV^2[i|t_r]$ are power functions of t_r .

44
$$E[i|t_r] = a_1 t_r^{b_1}$$
 (S5)

45
$$CV^2[i|t_r] = a_2 t_r^{b_2}$$
 (S6)

- The dependence is seasonally varying, which embodies in parameters a_1 and b_1 . The
- 47 values of b_1 and b_2 represent the extent of the dependence of $E[i|t_r]$ and
- 48 $CV^2[i|t_r]$ on t_r . The value of a_2 represents the correlation between the mean of
- 49 annual maximum rainfall intensity and t_r . The occurrence of extreme climate events
- may impact the average rainfall intensity.
- 51 The conditional distribution of i given t_r follows the gamma distribution:

52
$$f_I(i|t_r) = \frac{\lambda}{\Gamma(\kappa)} (\lambda i)^{\kappa - 1} exp(-\lambda i)$$
 (S7)

- According to (S5) and (S6), the gamma parameters κ and λ are estimated as the
- 54 functions of t_r as follows:

$$\kappa = \frac{t_r^{-b_2}}{a_2} \tag{S8}$$

$$56 \lambda = \frac{t_r^{-b_1 - b_2}}{a_1 a_2} (S9)$$

Combined with (S1), (S3), (S7), (S8), and (S9), the joint pdf of i and t_r is derived as

58 follows:

59
$$f_{I,T_r}(i,t_r|\gamma) = f_I(i|t_r)f_{T_r}(t_r|\gamma)$$
 (S10)

- 60 Third, constructing within-storm rainfall intensity variations using a normalized mass
- 61 curve (Huff, 1967; Chow et al., 1988):

62
$$H(t^*) = \frac{1}{it_r} \int_0^t i(t') dt'$$
 (S11)

- Where $t^* = t/t_r$ ($0 \le t^* \le 1$), i is the average rainfall intensity for the single storm,
- and i(t') is the instantaneous rainfall intensity at time t' within the certain storm
- 65 $(0 \le t' \le t_r)$. In order to generate realistic within-storm rainfall intensity patterns, a
- stochastic model capable of producing normalized mass curves satisfying the statistical
- 67 characteristic was developed to replace the equation above (referring to Robinson and
- 68 Sivapalan, [1997], section 3.4.2).

In order to elucidate the effect of inter-annual rainfall variability on N dynamic, 100 stochastic rainfall time series of WY, NY, and DY (EDY) were generated by the stochastic rainfall generator (Figure S1) to substitute for the rainfall data in the simulation period.

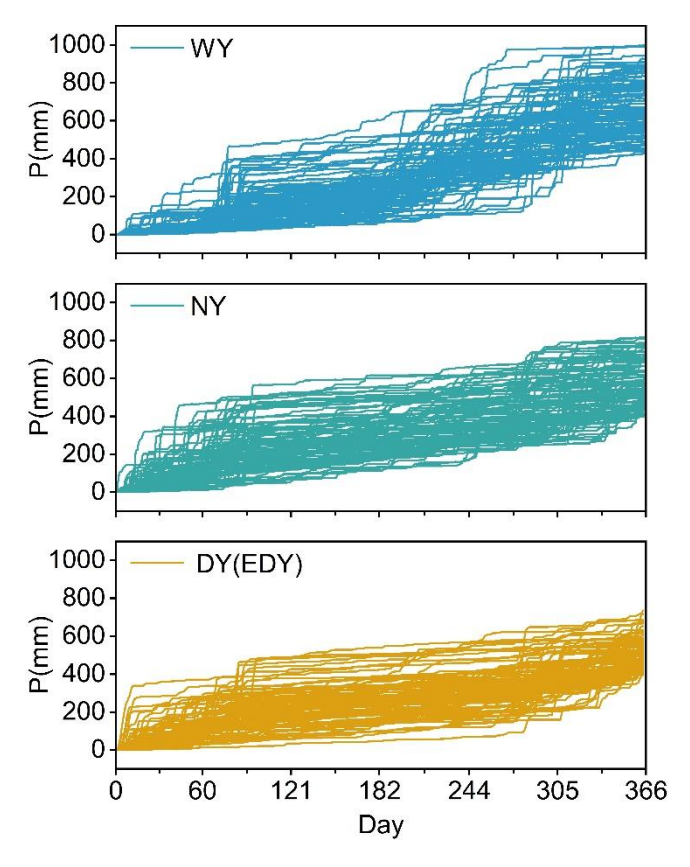
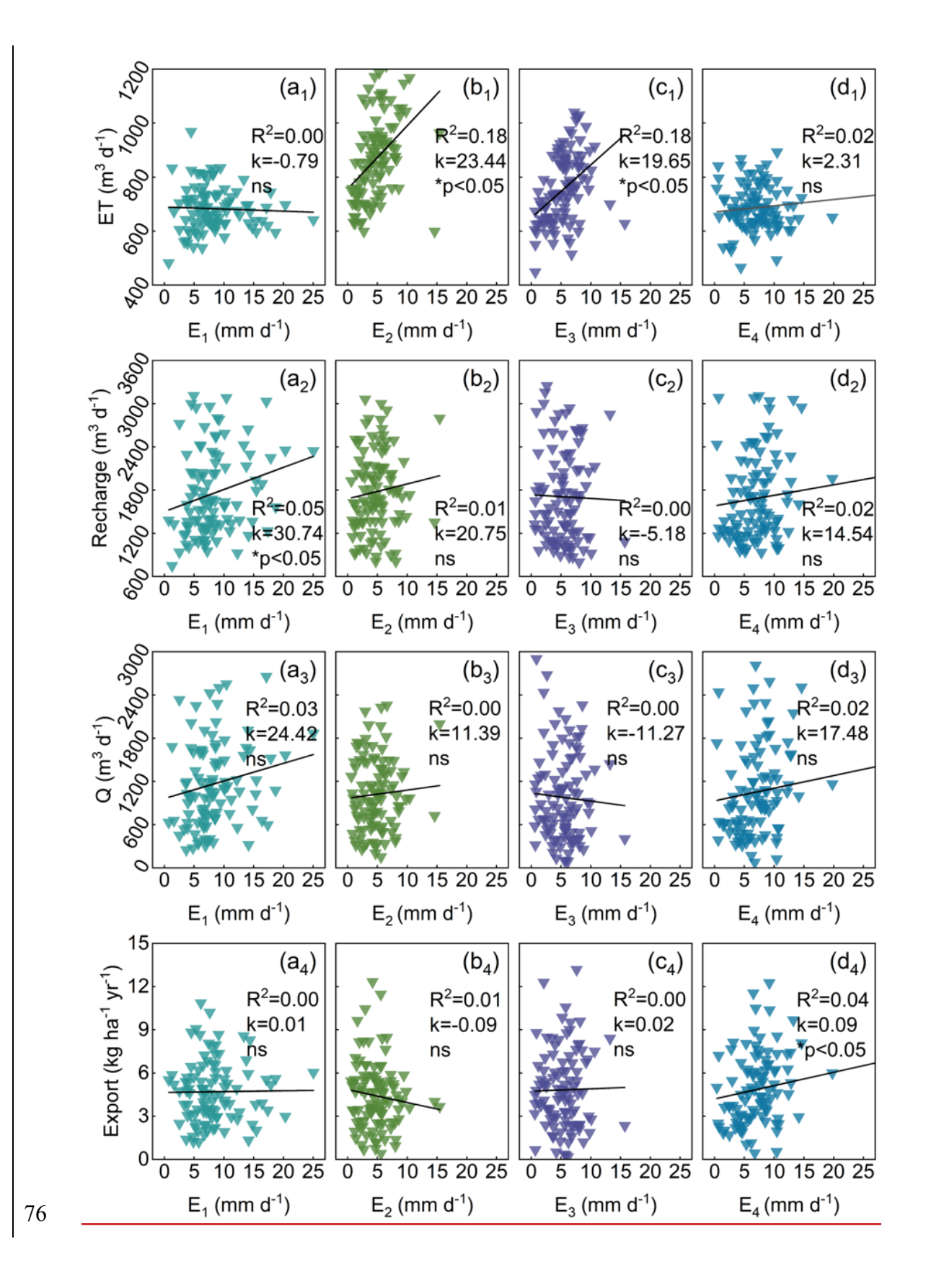


Figure S1. Daily cumulative values of 100 stochastic rainfall time series generated by the stochastic rainfall generator for WY, NY, and DY (EDY).



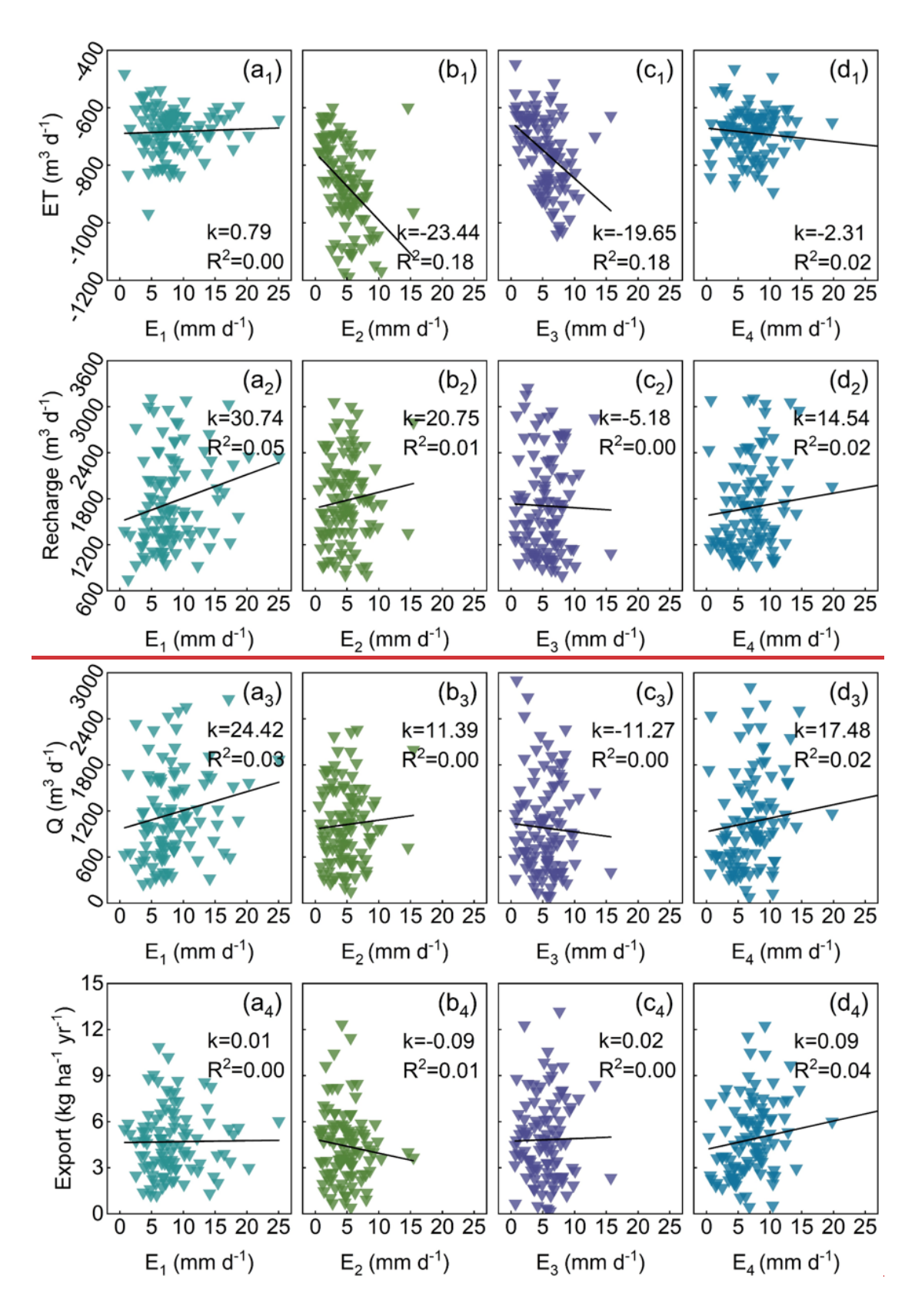


Figure S2. The responses of <u>actual</u> evapotranspiration (ET), recharge for groundwater, discharge (Q)₂ and N export to the average rainfall intensity of the four seasons (E₁-E₄). <u>The determination coefficients (R²) between E₁-E₄ and ET, Recharge, Q, and <u>as well as Eexport are listed.</u> The sign and magnitude of the slopes (k) in these linear relationships denote the</u>

- 82 direction and the intensity of the response of N dynamics to the variations in average rainfall
- intensity, respectively. Asterisks indicate the significance of the regression slopes (p < 0.05); ns
- 84 denotes non-significant relationships ($p \ge 0.05$). The determination coefficients (\mathbb{R}^2) between
- 85 E₁-E₄ and ET, Recharge, Q as well as Export are listed.